

Low surface brightness galaxies rotation curves in the low energy limit of R^n gravity : no need for dark matter ?

S. Capozziello¹, V.F. Cardone², A. Troisi¹

¹ *Dipartimento di Scienze Fisiche, Università degli studi di Napoli “Federico II” and INFN, Sezione di Napoli, Complesso Universitario di Monte S. Angelo, Via Cinthia, Edificio N, 80126 Napoli, Italy*

² *Dipartimento di Fisica “E.R. Caianiello”, Università di Salerno, Via S. Allende, 84081 - Baronissi (Salerno), Italy*

Accepted xxx, Received yyy, in original form zzz

ABSTRACT

We investigate the possibility that the observed flatness of the rotation curves of spiral galaxies is not an evidence for the existence of dark matter haloes, but rather a signal of the breakdown of General Relativity. To this aim, we consider power-law fourth order theories of gravity obtained by replacing the scalar curvature R with $f(R) = f_0 R^n$ in the gravity Lagrangian. We show that, in the low energy limit, the gravitational potential generated by a pointlike source may be written as $\Phi(r) \propto r^{-1} [1 + (r/r_c)^\beta]$ with β a function of the slope n of the gravity Lagrangian and r_c a scalelength depending on the gravitating system properties. In order to apply the model to realistic systems, we compute the modified potential and the rotation curve for spherically symmetric and for thin disk mass distributions. It turns out that the potential is still asymptotically decreasing, but the corrected rotation curve, although not flat, is higher than the Newtonian one thus offering the possibility to fit rotation curves without dark matter. To test the viability of the model, we consider a sample of 15 low surface brightness (LSB) galaxies with combined HI and H α measurements of the rotation curve extending in the putative dark matter dominated region. We find a very good agreement between the theoretical rotation curve and the data using only stellar disk and interstellar gas when the slope n of the gravity Lagrangian is set to the value $n = 3.5$ (giving $\beta = 0.817$) obtained by fitting the SNeIa Hubble diagram with the assumed power-law $f(R)$ model and no dark matter. The excellent agreement among theoretical and observed rotation curves and the values of the stellar mass-to-light ratios in agreement with the predictions of population synthesis models make us confident that R^n gravity may represent a good candidate to solve both the dark energy problem on cosmological scales and the dark matter one on galactic scales with the same value of the slope n of the higher order gravity Lagrangian.

Key words: gravitation – dark matter – galaxies: kinematics and dynamics – galaxies: low surface brightness

1 INTRODUCTION

An impressive amount of unprecedented high quality data have been accumulated in the last decade and have depicted the new picture of a spatially flat universe with a subcritical matter content and undergoing a phase of accelerated expansion. The measurements of cluster properties as the mass and correlation function and the evolution with redshift of their abundance (Eke et al. 1998; Viana et al. 2002; Bachall et al. 2003; Bachall & Bode 2003), the Hubble diagram of Type Ia Supernovae (Riess et al. 2004; Astier et al. 2006; Clocchiati et al. 2006), optical surveys of large scale

structure (Pope et al. 2005; Cole et al. 2005; Eisenstein et al. 2005), anisotropies in the cosmic microwave background (de Bernardis et al. 2000; Spergel et al. 2003), cosmic shear from weak lensing surveys (van Waerbeke et al. 2001; Refregier 2003) and the Lyman- α forest absorption (Croft et al. 1999; McDonald et al. 2005) are concordant evidences in favour of the radically new scenario depicted above. Interpreting this huge (and ever increasing) amount of information in the framework of a single satisfactory theoretical model is the main challenge of modern cosmology.

Although it provides an excellent fit to the most of the data (Tegmark et al. 2004; Seljak et al. 2005; Sanchez et

al. 2006), the old cosmological constant (Carroll et al. 1992; Sahni & Starobinski 2000) is affected by serious theoretical shortcomings that have motivated the search for alternative candidates generically referred to as *dark energy*. Rather than enumerating the many ideas on the ground (from a scalar field rolling down a suitably chosen self interaction potential to phantom fields and unified models of dark energy and dark matter), we refer the interested reader to the enlightening reviews available in literature (see, e.g., Peebles & Rathra 2003 and Padmanabhan 2003). Here, we only remind that dark energy acts as a negative pressure fluid whose nature and fundamental properties remain essentially unknown notwithstanding the great theoretical efforts made up to now.

Rather than being evidence for the need of some unknown component in the energy budget, the cosmic speed up of a low matter universe may also be considered as a first signal of breakdown of Einstein General Relativity. In this framework, higher order theories of gravity represent an interesting opportunity to explain cosmic acceleration without the need of any dark energy. In such models, the Ricci scalar curvature R in the gravity Lagrangian is replaced by a generic function $f(R)$ thus leading to modified Friedmann equations that can be formally written in the usual form by defining an effective negative pressure *curvature fluid* driving the cosmic acceleration (Capozziello 2002; Capozziello, Carloni and Troisi 2003; Carroll et al. 2004; Nojiri & Odintsov 2003). Also referred to as $f(R)$ theories, this approach has been extensively studied both from the theoretical (see, e.g., Capozziello, Cardone and Troisi 2005 and refs. therein) and observational point of view (Capozziello et al. 2003; Capozziello, Cardone and Francaviglia 2006; Borowiec, Godlowski and Szydowski 2006). Moreover, this same approach has been also proposed as a mechanism to give rise to an inflationary era without the need of any inflaton field (Starobinsky 1980). All these works have been concentrated on the cosmological applications of $f(R)$ theories and have convincingly demonstrated that they are indeed able to explain the cosmic speed up and fit the available dataset and hence represents a viable alternative to the mysterious dark energy.

Changing the gravity Lagrangian has consequences not only on cosmological scales, but also at the galactic ones so that it is mandatory to investigate the low energy limit of $f(R)$ theories. Unfortunately, here a strong debate is still open with different papers drawing contrasting results arguing in favour (Dick 2004; Sotiriou 2006; Cembranos 2006; Navarro & van Acoleyen 2005; Allemandi et al. 2005; Capozziello & Troisi 2005) or against (Dolgov 2003; Chiba 2003; Olmo 2005) such models. It is worth noting that, as a general result, higher order theories of gravity cause the gravitational potential to deviate from its Newtonian $1/r$ scaling (Stelle 1978; Kluske & Schmidt 1996; Schmidt 2004; Clifton & Barrow 2005; Sobouti 2006) even if such deviations may also be very soon vanishing.

In a previous paper (Capozziello et al. 2004), the Newtonian limit of power law $f(R) = f_0 R^n$ theories has been investigated, assuming that the metric in the low energy limit ($\Phi/c^2 \ll 1$) may be taken as Schwarzschild-like. It turns out that a power law term $(r/r_c)^\beta$ has to be added to the Newtonian $1/r$ term in order to get the correct gravitational potential. While the parameter β may be expressed analyti-

cally as function of the slope n of the $f(R)$ theory, r_c sets the scale where the correction term starts being significant and has to be determined case-by-case. We then investigated a particular range of values of n leading to $\beta > 0$ so that the corrective term is an increasing function of the radius r thus causing an increase of the rotation curve with respect to the Newtonian one and offering the possibility to fit the galaxy rotation curves without the need of the elusive dark matter component. As a preliminary test, we successfully fitted the Milky Way rotation curve using a model made out of the luminous components (bulge and disk) only. Notwithstanding these encouraging results, the corrected potential for n in the range explored in our previous paper is, however, troublesome. Indeed, the correction term never switches off so that the total gravitational potential has the unpleasant feature of being formally divergent as r goes to infinity. Actually, the expression for the gravitational potential has been obtained in the low energy limit so that cannot be extrapolated to distances where this approximation does not hold anymore. Nevertheless, for typical values of the parameters (β, r_c) , the rotation curve starts increasing for values of r near the visible edge of the disk thus contradicting what is observed in outer galaxies where the rotation curve is flat or slowly rising (Persic et al. 1996; Catinella et al. 2006).

Elaborating further on the previous results, we present here the analysis of the gravitational potential which is obtained by considering a different approach to the Newtonian limit of $f(R)$ theories giving rise to a correction term $(r/r_c)^\gamma$ with $-1 < \gamma < 0$. As we will see, the corresponding rotation curve is asymptotically decreasing as in the Newtonian case, but is nevertheless higher than the standard one so that it is still possible to fit the data without the need of dark matter. Moreover, for such models, the gravitational potential asymptotically vanishes so that the problem discussed above is avoided. To further substantiate our model, we consider a set of low surface brightness (hereafter LSB) galaxies with extended and well measured rotation curves. Since these systems are supposed to be dark matter dominated, successfully fitting our model with *no dark matter* to the LSB rotation curves would be a strong evidence in favor of our approach. Combined with the hints coming from the cosmological applications discussed above, we should thus have the possibility to solve both the dark energy and dark matter problems resorting to the same well motivated fundamental theory (see (Capozziello, Cardone and Troisi 2006) for preliminary results in this sense).

The plan of the paper is as follows. In Sect. 2, we briefly resume how the gravitational potential may be obtained in the low energy limit of power-law $f(R)$ theories in the case of a pointlike source. The generalization to both a spherically symmetric system and a thin disk is presented in Sect. 3. The data on the rotation curve, the modelling of LSB galaxies and the method adopted to determine the model parameters are presented in Sect. 4. An extensive analysis of the fitting procedure is carried out in Sect. 5 where we use simulated rotation curves to investigate how parameter degeneracies affect the estimate of the model parameters. The results of the fit are presented in Sect. 6, while Sect. 7 is devoted to summarize and foresee future prospects. Some more details on the fit results on a case-by-case basis and on the smoothing procedure are given in Appendix A and B respectively.

2 LOW ENERGY LIMIT OF $F(R)$ GRAVITY

As yet stated in the introduction, $f(R)$ theories of gravity represent a straightforward generalization of the Einstein General Relativity. To this aim, one considers the action :

$$A = \int d^4x \sqrt{-g} [f(R) + \mathcal{L}_m] \quad (1)$$

where $f(R)$ is a generic analytic function of the Ricci scalar curvature R and \mathcal{L}_m is the standard matter Lagrangian. The choice $f(R) = R + 2\Lambda$ gives the General Relativity including the contribution of the cosmological constant Λ . Varying the action with respect to the metric components $g_{\mu\nu}$, one gets the generalized Einstein equations that can be more expressively recast as (Capozziello 2002; Capozziello, Cardone and Troisi 2005) :

$$G_{\mu\nu} = \frac{1}{f'(R)} \left\{ \frac{1}{2} g_{\mu\nu} [f(R) - Rf'(R)] + f'(R)_{;\mu\nu} - g_{\mu\nu} \square f'(R) \right\} + \frac{T_{\mu\nu}^{(m)}}{f'(R)} \quad (2)$$

where $G_{\mu\nu} = R_{\mu\nu} - (R/2)g_{\mu\nu}$ is the Einstein tensor and the prime denotes derivative with respect to R . The two terms $f'(R)_{;\mu\nu}$ and $\square f'(R)$ imply fourth order derivatives of the metric $g_{\mu\nu}$ so that these models are also referred to as *fourth order gravity*. Starting from Eq.(2) and adopting the Robertson - Walker metric, it is possible to show that the Friedmann equations may still be written in the usual form provided that an *effective curvature fluid* (hence the name of *curvature quintessence*) is added to the matter term with energy density and pressure depending on the choice of $f(R)$. As a particular case, we consider power-law $f(R)$ theories, i.e. we set :

$$f(R) = f_0 R^n \quad (3)$$

with n the slope of the gravity Lagrangian ($n = 1$ being the Einstein theory) and f_0 a constant with the dimensions chosen in such a way to give $f(R)$ the right physical dimensions. It has been shown that the choice (3), with $n \neq 1$ and standard matter, is able to properly fit the Hubble diagram of Type Ia Supernovae without the need of dark energy (Capozziello et al. 2003; Carloni et al. 2005) and could also be reconciled with the constraints on the PPN parameters (Capozziello & Troisi 2005).

Here we study the low energy limit^{*} of this class of $f(R)$ theories. Let us consider the gravitational field generated by a pointlike source and solve the field equations (2) in the vacuum case. Under the hypothesis of weak gravitational fields and slow motions, we can write the spacetime metric as :

$$ds^2 = A(r)dt^2 - B(r)dr^2 - r^2 d\Omega^2 \quad (4)$$

where $d\Omega^2 = d\theta^2 + \sin^2\theta d\varphi^2$ is the line element on the unit sphere. It is worth noting that writing Eq.(4) for the weak field metric is the same as assuming implicitly that the Jebsen-Birkhoff theorem holds. While this is true in

^{*} Although not rigorously correct, in the following we will use the terms *low energy limit* and *Newtonian limit* as synonymous.

standard General Relativity, it has never been definitively proved for $f(R)$ theories. Actually, since for a general $f(R)$ theory the field equations are fourth order, it is quite difficult to show that the only stationary spherically symmetric vacuum solution is Schwarzschild like. However, that this is indeed the case has been demonstrated for $f(R)$ theories involving terms like $R + R^2$ with $R^2 = R_{\beta}^{\alpha\mu\nu} R_{\alpha}^{\beta\mu\nu}$ with torsion (Ramaswamy & Yasskin 1979) and for the case of any invariant of the form R^2 also in the case of null torsion (Neville 1980). Moreover, the Jebsen-Birkhoff theorem has been shown to hold also for more complicated theories as multidimensional gravity and Einstein-Yang-Mills theories (Brodbeck & Straumann 1993; Bronnikov & Melnikov 1995). Therefore, although a rigorous demonstration is still absent, it is likely that this theorem is still valid for power-law $f(R)$ theories, at least in an *approximated* weak version[†] that is enough for our aims.

To find the two unknown functions $A(r)$ and $B(r)$, we first combine the 00-vacuum component and the trace of the field equations (2) in absence of matter :

$$3\square f'(R) + Rf'(R) - 2f(R) = 0 ,$$

to get a single equation :

$$f'(R) \left(3 \frac{R_{00}}{g_{00}} - R \right) + \frac{1}{2} f(R) - 3 \frac{f'(R)_{;00}}{g_{00}} = 0 . \quad (5)$$

Eq.(5) is completely general and holds whatever is $f(R)$. It is worth stressing, in particular, that, even if the metric is stationary so that $\partial_t g_{\mu\nu} = 0$, the term $f'(R)_{;00}$ is not vanishing because of the non-null Christoffel symbols entering the covariant derivative. Using Eq.(3), Eq.(5) reduces to :

$$R_{00}(r) = \frac{2n-1}{6n} A(r)R(r) - \frac{n-1}{2B(r)} \frac{dA(r)}{dr} \frac{d \ln R(r)}{dr} , \quad (6)$$

while the trace equation reads :

$$\square R^{n-1}(r) = \frac{2-n}{3n} R^n(r) . \quad (7)$$

Note that for $n = 1$, Eq.(7) reduces to $R = 0$, which, inserted into Eq.(6), gives $R_{00} = 0$ and the standard Schwarzschild solution is recovered. In general, expressing R_{00} and R in terms of the metric (4), Eqs.(6) and (7) become a system of two nonlinear coupled differential equations for the two functions $A(r)$ and $B(r)$. A physically motivated hypothesis to search for solutions is

$$A(r) = \frac{1}{B(r)} = 1 + \frac{2\Phi(r)}{c^2} \quad (8)$$

with $\Phi(r)$ the gravitational potential generated by a pointlike mass m at the distance r . With the above hypothesis, the vacuum field equations reduce to a system of two differential equations in the only unknown function $\Phi(r)$. To be more precise, we can solve Eq.(6) or (7) to find out $\Phi(r)$ and then use the other relation as a constraint to find solutions of physical interest. To this aim, let us remember that, as

[†] It is, for instance, possible that the metric (4) solves the field equations only up to terms of low order in Φ/c^2 with Φ the gravitational potential. For the applications we are interested in, $\Phi/c^2 \ll 1$, such weak version of the Jebsen-Birkhoff theorem should be verified.

well known, $f(R)$ theories induces modifications to the gravitational potential altering the Newtonian $1/r$ scaling (Stelle 1978; Kluske & Schmidt 1996; Schmidt 2004; Clifton & Barrow 2005). We thus look for a solution for the potential that may be written as:

$$\Phi(r) = -\frac{Gm}{2r} \left[1 + \left(\frac{r}{r_c} \right)^\beta \right] \quad (9)$$

so that the gravitational potential deviates from the usual Newtonian one because of the presence of the second term on the right hand side. Note that, when $\beta = 0$, the Newtonian potential is recovered and the metric reduces to the classical Schwarzschild one. On the other hand, as we will see, it is just this term that offers the intriguing possibility to fit galaxy rotation curves without the need of dark matter.

In order to check whether Eq.(9) is indeed a viable solution, we first insert the expression for $\Phi(r)$ into Eqs.(6) and (7) which are both solved if:

$$(n-1)(\beta-3) \left[-\beta(1+\beta)V_1\eta^{\beta-3} \right]^{n-1} \times \left[1 + \frac{\beta V_1 \mathcal{P}_0}{\mathcal{P}_1 \eta} \right] \mathcal{P}_1 \eta = 0 \quad (10)$$

with $\eta = r/r_c$, $V_1 = Gm/c^2 r_c$ and

$$\begin{aligned} \mathcal{P}_0 &= 3(\beta-3)^2 n^3 - (5\beta^2 - 31\beta + 48)n^2 \\ &- (3\beta^2 - 16\beta + 17)n - (\beta^2 - 4\beta - 5), \end{aligned} \quad (11)$$

$$\begin{aligned} \mathcal{P}_1 &= 3(\beta-3)^2(1-\beta)n^3 + (\beta-3)^2(5\beta-7)n^2 \\ &- (3\beta^3 - 17\beta^2 + 34\beta - 36)n + (\beta^2 - 3\beta - 4)\beta. \end{aligned} \quad (12)$$

Eq.(10) is identically satisfied for particular values of n and β . However, there are some simple considerations allow to exclude such values. First, $n = 1$ must be discarded since, when deriving Eq.(6) from Eq.(5), we have assumed $R \neq 0$ which is not the case for $n = 1$. Second, the case $\beta = 3$ may also be rejected since it gives rise to a correction to the Newtonian potential scaling as η^2 so that the total potential diverges quadratically which is quite problematic. Finally, the case $\beta = -1$ provides a solution only if $n > 1$. Since we are interested in a solution which works whatever n is, we discard also this case. However, in the limit we are considering, it is $V_1 \ll 1$. For instance, it is $V_1 \simeq v_c^2/c^2 \sim 10^{-6} \div 10^{-3}$ ranging from Solar System to galactic scales, with v_c the circular velocity. As a consequence, we can look for a further solution of Eq.(10) solving:

$$\mathcal{P}_1(n, \beta)\eta + \beta V_1 \mathcal{P}_0(n, \beta) \simeq \mathcal{P}_1(n, \beta)\eta = 0. \quad (13)$$

since the second term of Eq.(13) is always negligible for the values of n and β in which we are interested. Eq.(13) is an algebraic equation for β as function of n with the following three solutions:

$$\beta = \begin{cases} \frac{3n-4}{n-1} \\ \frac{12n^2 - 7n - 1 - \sqrt{p(n)}}{q(n)} \\ \frac{12n^2 - 7n - 1 + \sqrt{p(n)}}{q(n)} \end{cases} \quad (14)$$

with:

$$p(n) = 36n^4 + 12n^3 - 83n^2 + 50n + 1,$$

$$q(n) = 6n^2 - 4n + 2.$$

It is easy check that, for $n = 1$, the second expression gives $\beta = 0$, i.e. the approximate solution reduces to the Newtonian one as expected. As a final check, we have inserted back into the vacuum field equations (5) and (7) the modified gravitational potential (9) with

$$\beta = \frac{12n^2 - 7n - 1 - \sqrt{36n^4 + 12n^3 - 83n^2 + 50n + 1}}{6n^2 - 4n + 2} \quad (15)$$

finding out that the approximated solution solve the field equations up to 10^{-6} which is more than sufficient in all astrophysical applications which we are going to consider.

Armed with Eqs.(9) and (15), we can, in principle, set constraints on n by imposing some physically motivated requirements to the modified gravitational potential. However, given the nonlinear relation between n and β , in the following we will consider β and use Eq.(15) to infer n from the estimated β .

As a first condition, it is reasonable to ask that the potential does not diverge at infinity. To this aim, we impose:

$$\lim_{r \rightarrow \infty} \Phi(r) = 0$$

which constraints $\beta - 1$ to be negative. A further constraint can be obtained considering the Newtonian potential $1/r$ as valid at Solar System scales. As a consequence, since the correction to the potential scales as $r^{\beta-1}$, we must impose $\beta - 1 > -1$ in order to avoid increasing Φ at the Solar System scales. In order to not evade these constraints, in the following, we will only consider solutions with

$$0 < \beta < 1 \quad (16)$$

that, using Eq.(15), gives $n > 1$ as lower limit on the slope n of the gravity Lagrangian.

While β controls the shape of the correction term, the parameter r_c controls the scale where deviations from the Newtonian potential sets in. Both β and r_c have to be determined by comparison with observations at galactic scales. An important remark is in order here. Because of Eq.(15), β is related to n which enters the gravity Lagrangian. Since this is the same for all gravitating systems, as a consequence, β must be the same for all galaxies. On the other hand, the scalelength parameter r_c is related to the boundary conditions and the mass of the system. In fact, considering the generalization of Eq.(9) to extended systems, one has to take care of the mass distribution and the geometrical configurations which can differ from one galaxy to another. As a consequence, r_c turns out to be not a universal quantity, but its value must be set on a case-by-case basis.

Before considering the generalization to extended systems, it is worth evaluating the rotation curve for the point-like case, i.e. the circular velocity $v_c(r)$ of a test particle in the potential generated by the point mass m . For a central potential, it is $v_c^2 = rd\Phi/dr$ that, with Φ given by Eq.(9), gives:

$$v_c^2(r) = \frac{Gm}{2r} \left[1 + (1-\beta) \left(\frac{r}{r_c} \right)^\beta \right]. \quad (17)$$

As it is apparent, the corrected rotation curve is the sum of two terms. While the first one equals half the Newtonian curve Gm/r , the second one gives a contribution that may also be higher than the half classical one. As expected, for $\beta = 0$, the two terms sum up to reproduce the classical result. On the other hand, for β in the range (16), $1 - \beta > 0$ so that the corrected rotation curve is higher than the Newtonian one. Since measurements of spiral galaxies rotation curves signal a circular velocity higher than what is predicted on the basis of the observed mass and the Newtonian potential, the result above suggests the possibility that our modified gravitational potential may fill the gap between theory and observations without the need of additional dark matter.

It is worth noting that the corrected rotation curve is asymptotically vanishing as in the Newtonian case, while it is usually claimed that observed rotation curves are flat (i.e., asymptotically constant). However, such a statement should be not be taken literally. Actually, observations do not probe v_c up to infinity, but only up to a maximum radius R_{max} showing that the rotation curve is flat within the measurement uncertainties. However, this by no way excludes the possibility that v_c goes to zero at infinity. Considering Eq.(17), if the exponent of the correction term is quite small, the first term decreases in a Keplerian way, while the second one approaches its asymptotically null value very slowly so that it can easily mimic an approximately flat rotation curve in agreement with observations.

3 EXTENDED SYSTEMS

The solution (9) has been obtained in the case of a pointlike source, but may be easily generalized to the case of extended systems. To this aim, we may simply divide the system in infinitesimal elements with mass dm and add the different contributions. In the continuous limit, the sum is replaced by an integral depending on the mass density and the symmetry of the system spatial configuration. Once the gravitational potential has been obtained, the rotation curve may be easily evaluated and then compared with observations.

3.1 Spherically symmetric systems

The generalization of Eq.(9) to a spherically symmetric system is less trivial than one would expect. In the case of the Newtonian gravitational potential, the Gauss theorem ensures us that the flux of the gravitational field generated by a point mass m through a closed surface only depends on the mass m and not on the position of the mass inside the surface. Moreover, the force on a point inside the surface due to sources outside the surface vanishes. As a result, we may imagine that the whole mass of the system is concentrated in its centre and, as a consequence, the gravitational potential has the same formal expression as for the pointlike case provided one replaces m with $M(r)$, being this latter quantity the mass within a distance r from the centre.

From a mathematical point of view, we can write in the Newtonian case :

$$\Phi_N(r) = -G \int \frac{\rho(\mathbf{x}')}{|\mathbf{x} - \mathbf{x}'|} d^3x'$$

$$\begin{aligned} &= -\frac{4\pi G}{r} \int_0^\infty \rho(r') r'^2 dr' \\ &= -\frac{GM(r)}{r} \end{aligned}$$

where, in the second row, we have used the Gauss theorem to take the $|\mathbf{x} - \mathbf{x}'|^{-1}$ outside the integral sign (considering all the mass concentrated in the point $\mathbf{x}' = 0$) and then limited the integral to r since points with $r' > r$ do not contribute to the gravitational force.

It is quite easy to show that the Gauss theorem for the gravitational field is a consequence of the scaling $1/r^2$ of the Newtonian force. Since this scaling is lost in the case of the modified potential (9), the Gauss theorem does not hold anymore. However, apart from the multiplicative factor $1/2$, we can split the modified gravitational potential as the sum of two terms, the first one scaling as in the Newtonian case. For this term, the Gauss theorem holds and we recover the classical results so that the total gravitational potential of a spherically symmetric system may be written as :

$$\Phi(r) = \frac{\Phi_N(r) + \Phi_c(r)}{2} = -\frac{GM(r)}{2r} + \frac{\Phi_c(r)}{2} \quad (18)$$

with :

$$\Phi_c(r) = -G \int_0^\infty \rho(r') r'^2 dr' \int_{-\pi/2}^{\pi/2} \sin \theta' d\theta' \int_0^{2\pi} \psi_c d\phi' \quad (19)$$

with ψ_c the non-Newtonian part of the modified gravitational potential for the pointlike case. In order to be more general, we consider the calculation for a generic modified potential of the type :

$$\psi = -\frac{Gm}{2r} \left[1 + \alpha \left(\frac{r}{r_c} \right)^\beta \right] \quad (20)$$

so that :

$$\psi_c(r) = -\frac{\alpha Gm}{r_c} \left(\frac{r}{r_c} \right)^{\beta-1} \quad (21)$$

with α and β two parameters depending on the particular theory of gravity one is considering. While for R^n gravity $\alpha = 1$, in general, α could also be negative. Inserting the above ψ_c into Eq.(19), we replace r' with

$$|\mathbf{x} - \mathbf{x}'| = (r^2 + r'^2 - 2rr' \cos \theta')^{1/2}$$

where we have used the spherical symmetry of the system so that the potential in the point $\mathbf{x} = (r, \theta, \phi)$ only depends on r and we can set $\theta = \phi = 0$. Integrating over the angular variables (θ', ϕ') , we finally get :

$$\Phi_c(r) = -\frac{\pi G \alpha r_c^2}{3} [\mathcal{I}_1(r) + \mathcal{I}_2(r)] \quad (22)$$

with :

$$\begin{aligned} \mathcal{I}_1 &= 3\pi \int_0^\infty (\xi^2 + \xi'^2)^{(\beta-1)/2} \rho(\xi') \xi'^2 d\xi' \\ &\times {}_2F_1 \left[\left\{ \frac{1-\beta}{4}, \frac{3-\beta}{4} \right\}, \{2\}, \frac{4\xi^2 \xi'^2}{(\xi^2 + \xi'^2)^2} \right], \quad (23) \end{aligned}$$

$$\begin{aligned} \mathcal{I}_2 &= 4(1-\beta) \xi \int_0^\infty (\xi^2 + \xi'^2)^{(\beta-3)/2} \rho(\xi') \xi'^2 d\xi' \\ &\times {}_3F_2 \left[\left\{ 1, \frac{3-\beta}{4}, \frac{5-\beta}{4} \right\}, \left\{ \frac{3}{2}, \frac{5}{2} \right\}, \frac{4\xi^2 \xi'^2}{(\xi^2 + \xi'^2)^2} \right] \quad (24) \end{aligned}$$

and we have generically defined $\xi = r/r_c$ and used the notation ${}_pF_1[\{a_1, \dots, a_p\}, \{b_1, \dots, b_q\}, x]$ for the hypergeometric functions.

Eqs.(23) and (24) must be evaluated numerically for a given expression of the mass density $\rho(r)$. Once $\Phi_c(r)$ has been evaluated, we can compute the rotation curve as:

$$v_c^2(r) = r \frac{\partial \Phi}{\partial r} = \frac{v_{c,N}^2(r)}{2} + \frac{r}{2} \frac{\partial \Phi_c}{\partial r} \quad (25)$$

with $v_{c,N}^2(r) = GM(r)/r$ the Newtonian rotation curve. Since we are mainly interested in spiral galaxies without any spherical component, we do not evaluate the rotation curve explicitly. We only note that, since Φ_c has to be evaluated numerically, in order to avoid numerical derivatives, it is better to first differentiate analytically the expressions for \mathcal{I}_1 and \mathcal{I}_2 and then integrate numerically the corresponding integrals. It is easy to check that the resulting rotation curve is typically slowly decreasing so that it vanishes asymptotically as in the Newtonian case. However, the rate of decline is slower than the Keplerian one so that the total rotation curve turns out to be higher than the Newtonian one: this fact allows to fit galaxy rotation curves without the need of any dark matter halo[‡].

3.2 Thin disk

The case of a disk-like system is quite similar to the previous one and, indeed, the gravitational potential may be determined following the same method as before simply taking care of the cylindrical rather than spherical symmetry of the mass configuration. In order to simplify computations, but still dealing with realistic systems, we will consider a circularly symmetric and infinitesimally thin disk and denote by $\Sigma(R)$ its surface mass density[§] and by R_d its scale length. Note that a thin circular disk is the standard choice in describing spiral galaxies so that the model we consider is indeed the most realistic one.

Adopting cylindrical coordinates (R, ϕ, z) , the gravitational potential may be evaluated as:

$$\Phi(R, z) = \int_0^\infty \Sigma(R') R' dR' \int_0^{2\pi} \psi(|\mathbf{x} - \mathbf{x}'|) d\phi' \quad (26)$$

with ψ the pointlike potential and:

$$|\mathbf{x} - \mathbf{x}'|^2 = [(R + R')^2 + z^2] [1 - k^2 \cos^2(\phi'/2)] \quad (27)$$

$$k^2 \equiv \frac{4RR'}{[(R + R')^2 + z^2]} \quad (28)$$

Inserting Eq.(20) into Eq.(26), we get an integral that can be split into two additive terms. The first one is half the usual Newtonian one that can be solved using standard procedure (Binney & Tremaine 1987) and therefore will not be

[‡] It is worth stressing, at this point, that general conservation laws are guaranteed by Bianchi identities which hold for generic $f(R)$, so the non-validity of Gauss theorem is not a shortcoming since we are considering the low energy limit of the theory.

[§] Here, R is the cylindrical coordinate in the plane of the disk (i.e., $R^2 = x^2 + y^2$) to be not confused with the Ricci scalar curvature.

considered anymore. The second one is the correction term Φ_c that reads[¶]:

$$\begin{aligned} \Phi_c(R, z) &= -\alpha G \Sigma_0 r_c \int_0^\infty \tilde{\Sigma}(\xi') [(\xi + \xi')^2 + \zeta^2]^{\frac{\beta-1}{2}} \xi' d\xi' \\ &\times \int_0^{2\pi} [1 - k^2 \cos^2(\phi'/2)]^{\frac{\beta-1}{2}} d\phi' \end{aligned} \quad (29)$$

with $\Sigma_0 = \Sigma(R=0)$, $\tilde{\Sigma} = \Sigma/\Sigma_0$, $\xi = R/r_c$ and $\zeta = z/r_c$. Integrating over $d\phi'$ and using Eq.(28), we finally get:

$$\begin{aligned} \Phi_c(R, z) &= -2^{\beta-2} \pi \alpha G \Sigma_0 r_c \xi^{\frac{\beta-1}{2}} \int_0^\infty d\xi' \tilde{\Sigma}(\xi') \xi'^{\frac{1+\beta}{2}} \\ &\times {}_2F_1 \left[\left\{ \frac{1}{2}, \frac{1-\beta}{2} \right\}, \{1\}, k^2 \right] k^{1-\beta}. \end{aligned} \quad (30)$$

Eq.(30) makes it possible to evaluate the corrective term to the gravitational potential generated by an infinitely thin disk given its surface density $\Sigma(\xi)$. As a useful application, we consider the case of the exponential disk (Freeman 1970):

$$\Sigma(R) = \Sigma_0 \exp(-R/R_d) \quad (31)$$

with R_d the scale radius. With this expression for the surface density, the corrective term in the gravitational potential may be conveniently written as:

$$\begin{aligned} \Phi_c(R, z) &= -2^{\beta-2} \eta_c^{-\beta} \pi \alpha G \Sigma_0 R_d \eta^{\frac{\beta-1}{2}} \int_0^\infty d\eta' e^{-\eta'} \eta'^{\frac{\beta+1}{2}} \\ &\times {}_2F_1 \left[\left\{ \frac{1}{2}, \frac{1-\beta}{2} \right\}, \{1\}, k^2 \right] k^{1-\beta} \end{aligned} \quad (32)$$

with $\eta = R/R_d$ and $\eta_c = r_c/R_d$ and k is still given by Eq.(28) replacing (R, R', z) with $(\eta, \eta', z/R_d)$. The rotation curve for the disk may be easily computed starting from the usual relation (Binney & Tremaine 1987):

$$v_c^2(R) = R \frac{\partial \Phi(R, z)}{\partial R} \Big|_{z=0} = \eta \frac{\partial \Phi(R, z)}{\partial \eta} \Big|_{z/R_d=0} \quad (33)$$

Inserting the total gravitational potential into Eq.(33), we may still split the rotation curve in two terms as:

$$v_c^2(R) = \frac{v_{c,N}^2(R) + v_{c,corr}^2(R)}{2} \quad (34)$$

where the first term is the Newtonian one, which for an exponential disk reads (Freeman 1970):

$$\begin{aligned} v_{c,N}^2(R) &= 2\pi G \Sigma_0 R_d (\eta/2)^2 \\ &\times [I_0(\eta/2) K_0(\eta/2) - I_1(\eta/2) K_1(\eta/2)] \end{aligned} \quad (35)$$

with I_l, K_l Bessel functions of order l of the first and second type respectively. The correction term $v_{c,corr}^2$ may be evaluated inserting Eq.(32) into Eq.(33). Using:

$$\frac{\partial k}{\partial \eta} = \frac{k}{2\eta} \left[1 - \frac{k^2(\eta + \eta')}{2\eta'} \right],$$

we finally get:

[¶] As in the previous paragraph, it is convenient to let apart the multiplicative factor $1/2$ and insert it only in the final result so that the total potential reads $\Phi(R, z) = [\Phi_N(R, z) + \Phi_c(R, z)]/2$.

$$v_{c,corr}^2(\eta) = -2^{\beta-5} \eta_c^{-\beta} \pi \alpha (\beta - 1) G \Sigma_0 R_d \eta^{\frac{\beta-1}{2}} \mathcal{I}_{disk}(\eta, \beta) \quad (36)$$

where we have defined :

$$\mathcal{I}_{disk}(\eta, \beta) = \int_0^\infty \mathcal{F}(\eta, \eta', \beta) k^{3-\beta} \eta'^{\frac{\beta-1}{2}} e^{-\eta'} d\eta' \quad (37)$$

with :

$$\begin{aligned} \mathcal{F} = & 2(\eta + \eta') {}_2F_1 \left[\left\{ \frac{1}{2}, \frac{1-\beta}{2} \right\}, \{1\}, k^2 \right] \\ & + \left[(k^2 - 2)\eta' + k^2\eta \right] {}_2F_1 \left[\left\{ \frac{3}{2}, \frac{3-\beta}{2} \right\}, \{2\}, k^2 \right]. \end{aligned} \quad (38)$$

The function $\mathcal{I}_{disk}(\eta, \beta)$ may not be evaluated analytically, but it is straightforward to estimate it numerically. Note that Eqs.(36) and (37) can be easily generalized to a different surface density by replacing the term $e^{-\eta'}$ with $\tilde{\Sigma}(\eta')$ and R_d with R_s , being this latter a typical scale radius of the system, while the function \mathcal{F} remains unaltered.

4 LSB ROTATION CURVES

Historically, the flatness of rotation curves of spiral galaxies was the first and (for a long time) more convincing evidence for the existence of dark matter (Sofue & Rubin 2001). Despite much effort, however, it is still unclear to what extent bright spiral galaxies may give clues about the properties of the putative dark haloes. On the one hand, being poor in gas content, their rotation curves is hardly measured out to very large radii beyond the optical edge of the disk where dark matter is supposed to dominate the rotation curve. On the other hand, the presence of extended spiral arms and barred structures may lead to significative non-circular motions thus complicating the interpretation of the data. On the contrary, LSB and dwarf galaxies are supposed to be dark matter dominated at all radii so that the details of the visible matter distribution are less important. In particular, LSB galaxies have an unusually high gas content, representing up to 90% of their baryonic content (van den Hock et al. 2000; Schombert et al. 2001), which makes it possible to measure the rotation curve well beyond the optical radius $R_{opt} \simeq 3.2R_d$. Moreover, combining 21 - cm HI lines and optical emission lines such as H α and [NII] makes it possible to correct for possible systematic errors due to beam smearing in the radio. As a result, LSB rotation curves are nowadays considered a useful tool to put severe constraints on the properties of the dark matter haloes (see, e.g., de Blok 2005 and references therein).

4.1 The data

It is easy to understand why LSB rotation curves are ideal tools to test also modified gravity theories. Indeed, successfully fitting the rotation curves of a whatever dark matter dominated system, without resorting to dark matter, should represent a serious evidence arguing in favour of modifications of the standard Newtonian potential. In order to test our model, we have therefore considered a sample of 15 LSB galaxies with well measured HI and H α rotation curves extracted from a larger sample in de Blok & Bosma (2002). The initial sample contains 26 galaxies, but we have only considered those galaxies for which data on the rotation curves, the

Table 1. Properties of sample galaxies. Explanation of the columns: name of the galaxy, distance in Mpc; disk central surface brightness in the R band (corrected for galactic extinction); disk scalelength in kpc; radius at which the gas surface density equals $1 \text{ M}_\odot/\text{pc}^2$ in arcsec; total HI gas mass in 10^8 M_\odot ; Hubble type as reported in the NED database.

Id	D	μ_0	R_d	R_{HI}	M_{HI}	Type
UGC 1230	51	22.6	4.5	101	58.0	Sm
UGC 1281	5.5	22.7	1.7	206	3.2	Sdm
UGC 3137	18.4	23.2	2.0	297	43.6	Sbc
UGC 3371	12.8	23.3	3.1	188	12.2	Im
UGC 4173	16.8	24.3	4.5	178	21.2	Im
UGC 4325	10.1	21.6	1.6	142	7.5	SAm
NGC 2366	3.4	22.6	1.5	439	7.3	IB(s)m
IC 2233	10.5	22.5	2.3	193	13.6	SBd
NGC 3274	6.7	20.2	0.5	225	6.6	SABd
NGC 4395	3.5	22.2	2.3	527	9.7	SAm
NGC 4455	6.8	20.8	0.7	192	5.4	SBd
NGC 5023	4.8	20.9	0.8	256	3.5	Scd
DDO 185	5.1	23.2	1.2	136	1.6	IBm
DDO 189	12.6	22.6	1.2	167	10.5	Im
UGC 10310	15.6	22.0	1.9	130	12.6	SBm

surface photometry in the R band and the gas mass surface density were available^{||}. In Table 1, we report the quantities we need for evaluating the theoretical rotation curve referring the reader to de Blok & Bosma (2002) for further details and references to retrieve the data^{**}.

An important remark in order here. For each LSB galaxy, both HI and H α data on the rotation curve are available. As yet discussed in de Blok & Bosma (2002), the raw data show some scatter mainly due to residuals non circular motions that may lead to ambiguous rotational velocities. However, when deriving mass models from rotation curves, each galaxy is described as an axisymmetric system so that non circular motions do not arise. In order to remove this scatter from the data, it is recommended to use the smoothed rotation curve data derived by a local regression method extensively discussed in de Blok & Bosma (2002 and refs. therein). Following these authors, we will adopt the smooth data as input in the fitting procedure. The smoothing procedure may in principle introduce correlations among the data so that it is worth investigating whether this may bias somewhat the results on the model parameters. Moreover, the number of data points on each single rotation curve is reduced and the errors on each point is estimated in a different way than for raw data. As such, it is important to investigate also how this affects the uncertainties on the final estimate of the model parameters.

^{||} This initial selection reduced indeed the sample to 19 galaxies, but four of them were rejected because of numerical problems when computing the gas rotation curve due to the strong irregularities in the interpolated surface density.

^{**} The data on the rotation curves may be also found in the SIMBAD database (<http://cdsweb.u-strasbg.fr>).

4.2 Modelling LSB galaxies

Since we are interested in fitting rotation curves without any dark matter halo, our model for a generic LSB galaxy is made out of the stellar and gaseous components only.

We assume the stars are distributed in an infinitely thin and circularly symmetric disk. The surface density $\Sigma(R)$ may be derived from the surface brightness distribution :

$$\mu(R) = -2.5 \log I(R)$$

with $I(R) = \Sigma(R)/\Upsilon_*$ the light distribution and Υ_* the stellar mass-to-light (hereafter M/L) ratio. The photometric data (in the R band) are fitted with an exponential model thus allowing to determine the scalelength R_d and the central surface brightness μ_0 and hence $I_0 = I(R=0)$. The only unknown parameter is therefore Υ_* that makes it possible to convert the central luminosity density I_0 into the central surface mass density Σ_0 entering Eqs.(35) and (36).

Modelling the gas distribution is quite complicated. Following the standard practice, we assume the gas is distributed in a infinitely thin and circularly symmetric disk assuming for the surface density $\Sigma(R)$ the profile that has been measured by the HI 21-cm lines. Since the measurements only cover the range $R_{min} \leq R \leq R_{max}$, we use a third order interpolation for R in this range, a linear extrapolation between R_{max} and R_{HI} , being this latter a scaling radius defined by $\Sigma(R_{HI}) = 1 \text{ M}_\odot/\text{pc}^2$, while we assume $\Sigma(R) = \Sigma(R_{min})$ for $R \leq R_{min}$. To check if the model works correctly, we compute the total mass M_{HI} and normalize the model in such a way that this value is the same as that is measured by the total HI 21-cm emission. Finally, we increase the surface mass density by 1.4 to take into account the helium contribution. It is worth noting that our model is only a crude approximation for R outside the range (R_{min}, R_{max}) , while, even in the range (R_{min}, R_{max}) , $\Sigma(R)$ gives only an approximated description of the gas distribution since this latter may be quite clumpy and therefore cannot be properly fitted by any analytical expression. We stress, however, that the details of the gas distribution are rather unimportant since the rotation curve is dominated everywhere by the stellar disk. The clumpiness of the gas distribution manifests itself in irregularities in the rotation curve that may be easily masked in the fitting procedure, even if this is not strictly needed for our aims.

4.3 Fitting the rotation curve

Having modelled a LSB galaxy, Eqs.(35)–(38) may be straightforwardly used to estimate the theoretical rotation curve as function of three unknown quantities, namely the stellar M/L ratio Υ_* and the two theory parameters (β, r_c) . Actually, we will consider as fitting parameters $\log r_c$ rather than r_c (in kpc) since this is a more manageable quantity that makes it possible to explore a larger range for this theoretically unconstrained parameter. Moreover, we use the gas mass fraction f_g rather than Υ_* as fitting quantity since the range for f_g is clearly defined, while this is not for Υ_* . The two quantities are easily related as follows :

$$f_g = \frac{M_g}{M_g + M_d} \iff \Upsilon_* = \frac{(1 - f_g)M_g}{f_g L_d} \quad (39)$$

with $M_g = 1.4M_{HI}$ the gas (HI + He) mass, $M_d = \Upsilon_* L_d$ and $L_d = 2\pi I_0 R_d^2$ the disk total mass and luminosity.

We use Eq.(35) to compute the disk Newtonian rotation curve, while the $v_{c,corr}$ is obtained by integrating numerically Eq.(37). For the gas, instead, we resort to numerical integrations for both the Newtonian rotation curve and the corrective term. The total rotation curve is finally obtained by adding in quadrature these contributions.

To constrain the parameters $(\beta, \log r_c, f_g)$, we minimize the following merit function :

$$\chi^2(\mathbf{p}) = \sum_{i=1}^N \left[\frac{v_{c,th}(r_i) - v_{c,obs}(r_i)}{\sigma_i} \right]^2 \quad (40)$$

where the sum is over the N observed points. While using the smoothed data helps in better adjusting the theoretical and observed rotation curves, the smoothing procedure implies that the errors σ_i on each point are not Gaussian distributed since they also take into account systematic misalignments between HI and $H\alpha$ measurements and other effects leading to a conservative overestimate of the true uncertainties (see the discussion in (de Blok & Bosma 2002) for further details). As a consequence, we do not expect that $\chi^2/dof \simeq 1$ for the best fit model (with $dof = N - 3$ the number of degrees of freedom), but we can still compare different models on the basis of the χ^2 values. In particular, the uncertainties on the model parameters will be estimated exploring the contours of equal $\Delta\chi^2 = \chi^2 - \chi^2_{min}$ in the parameter space.

5 TESTING THE METHOD

The method we have outlined above and the data on LSB galaxies are in principle all what we need to test the viability of R^n gravity. However, there are some subtle issues that can affect in an unpredictable way the outcome of the analysis.

Two main problems worth to be addressed. First, there are three parameters to be constrained, namely the gas mass fraction f_g (related to the stellar M/L ratio Υ_*) and the R^n gravity quantities $(\beta, \log r_c)$. However, although they do not affect the theoretical rotation curve in the same way, there are still some remaining degeneracies hard to be broken. This problem is well illustrated by Fig.,1 where we show the contours of equal $v_c(R_d)$ in the planes $(\beta, \log r_c)$, (β, f_g) and $(\log r_c, f_g)$ for the pointlike and extended case. Looking, for instance, at right panels, one sees that, for a given β , $\log r_c$ and f_g (and hence Υ_*) have the same net effect on the rotation curve so that the same value for $v_c(R_d)$ may be obtained for a lower f_g provided one increases $\log r_c$. On the other hand, β and $\log r_c$ have opposite effects on $v_c(R)$: the lower is β , the smaller is $v_c(R)$ for a given R . Since the opposite holds for $\log r_c$, as a result, the same value of $v_c(R_d)$ may be obtained increasing $\log r_c$ and decreasing β . Moreover, while β drives the shape of the rotation curve in the outer region, its effect may be better appreciated if r_c is low so that a further degeneracy arises.

A second issue is related to our decision to use the smooth rather than the raw data. Although de Blok & Bosma (2002) claim that this does not affect the results, their analysis is nevertheless performed in the framework of standard theory of gravity with dark matter haloes. It is

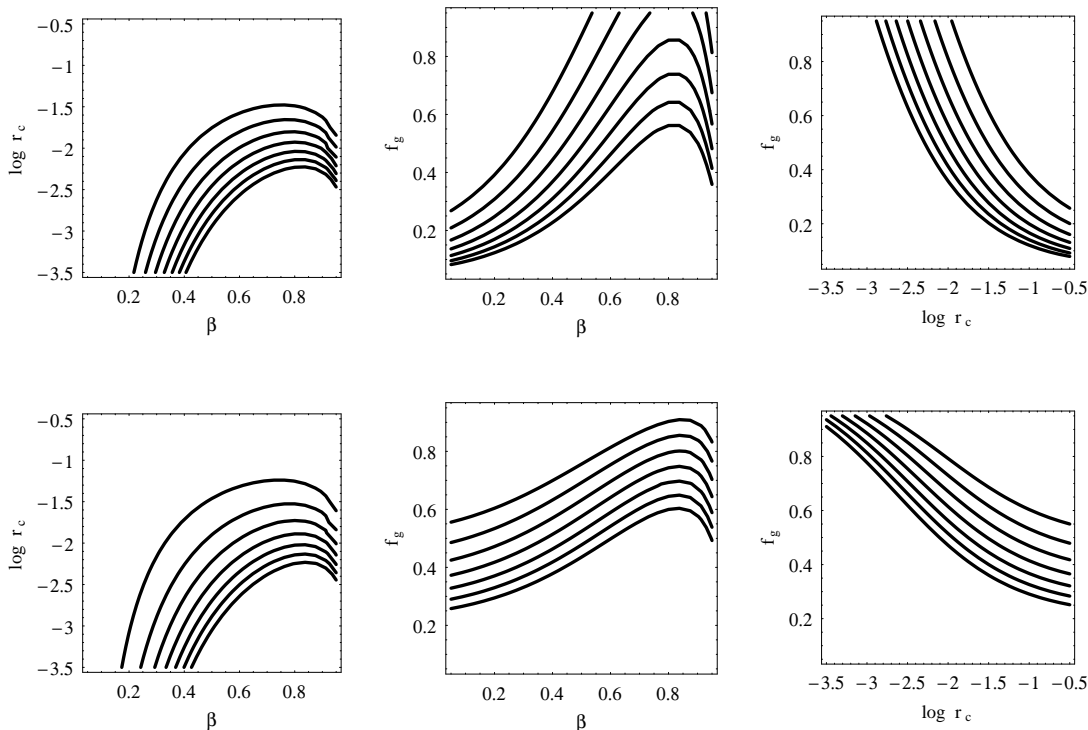


Figure 1. Contour plots for $v_c(R_d)$ in the planes $(\beta, \log r_c)$, (left), (β, f_g) (middle), $(\log r_c, f_g)$ (right) with r_c in kpc. The contours are plotted for $v_c(R) = k \times v_{fid}$ with k from 0.7 to 1.3 in steps of 0.1 and $v_{fid} = v_c(R_d)$ for the model with $(\beta, \log r_c, f_g) = (0.61, -2.13, 0.65)$. Upper panels refer to a pointlike system with total mass $m = \Upsilon_* L_d + M_{HI}$, with L_d the total disk luminosity, M_{HI} the gas mass and Υ_* given by Eq.(39). Lower panels refer to the extended case using as default parameters those of UGC 10310. In each panel, the remaining parameter is set to its fiducial value. Note that similar plots are obtained for values of R other than R_d .

therefore worth investigating whether this holds also in the case of the R^n gravity we are considering here.

Both these issues may be better investigated through the analysis of simulated rotation curves. To this aim, we take UGC 10310 as input model for the gas surface density and the disk luminosity because its properties are typical of our sample. For given values of the model parameters $(\beta, \log r_c, f_g)$, we generate observed rotation curves using the same radial sampling of the actual observations. For each r_i , we randomly extract $v_{c,obs}(r_i)$ from a Gaussian distribution centred on the $v_{c,th}(r_i)$. To this point, we attach an error extracted from a second Gaussian distribution centred on the $\varepsilon_i \times v_{c,obs}(r_i)$ with ε_i the percentage error on $v_{c,obs}(r_i)$ in the real sample. The simulated rotation curves thus obtained are quite similar to the raw data so that we use the same smoothing procedure (as in Appendix B) to get simulated smooth data. Both the simulated raw and smooth data are quite similar to the corresponding observed ones so that they represent ideal tools to explore the issues quoted above.

5.1 The impact of the parameters degeneracy

As well known, the determination of \mathcal{N} model parameters from the fit to a given dataset may be seriously compromised if strong degeneracies exist. Considering for simplicity the case of a pointlike source, the rotation curve may be roughly approximated as :

$$v_c^2(r) \simeq \frac{Gm}{2r} \times \begin{cases} 1 & \text{for } (r/r_c)^\beta \ll 1 \\ 1 + (1 - \beta) & \text{for } (r/r_c)^\beta \simeq 1 \\ (1 - \beta)(r/r_c)^\beta & \text{for } (r/r_c)^\beta \gg 1 \end{cases} .(41)$$

For the typical values of β (~ 0.8) and r_c ($\simeq 0.01$ kpc) we qualitatively estimate from an eyeball fit to the data, it is easy to check that most of the data in the rotation curves mainly probe the region with $(r/r_c)^\beta \gg 1$ so that $v_c^2 \simeq Gm/2r_c \times (1 - \beta)(r/r_c)^{\beta-1}$. As a result, the theoretical rotation curve mainly depends on the two effective parameters $m_{eff} = m(1 - \beta)/2$ and $r_{c,eff} = r_c^\beta$. Moreover, as a further complication, the lower is β , the less v_c^2 depends on r_c since the correction term is more and more negligible. A similar discussion (although less intuitively) also holds in the extended case with the stellar M/L ratio Υ_* playing the role of the pointlike mass m . Both these problems may be better appreciated looking at Fig. 1 as yet discussed above. It is therefore mandatory to explore whether the data are able to break these degeneracies or how they affect the recovering of the model parameters $(\beta, \log r_c, f_g)$.

This task may be ideally tackled fitting the simulated rotation curves generated as described above and comparing the best fit values with the input ones. Indeed, we find that the degeneracy works in a quite dramatic way possibly leading to large discrepancies among the input and best fit values. To better illustrate this point, some typical examples have been reported in Fig. 2 where the input theoretical rotation curve (solid line) and the best fit one (short dashed

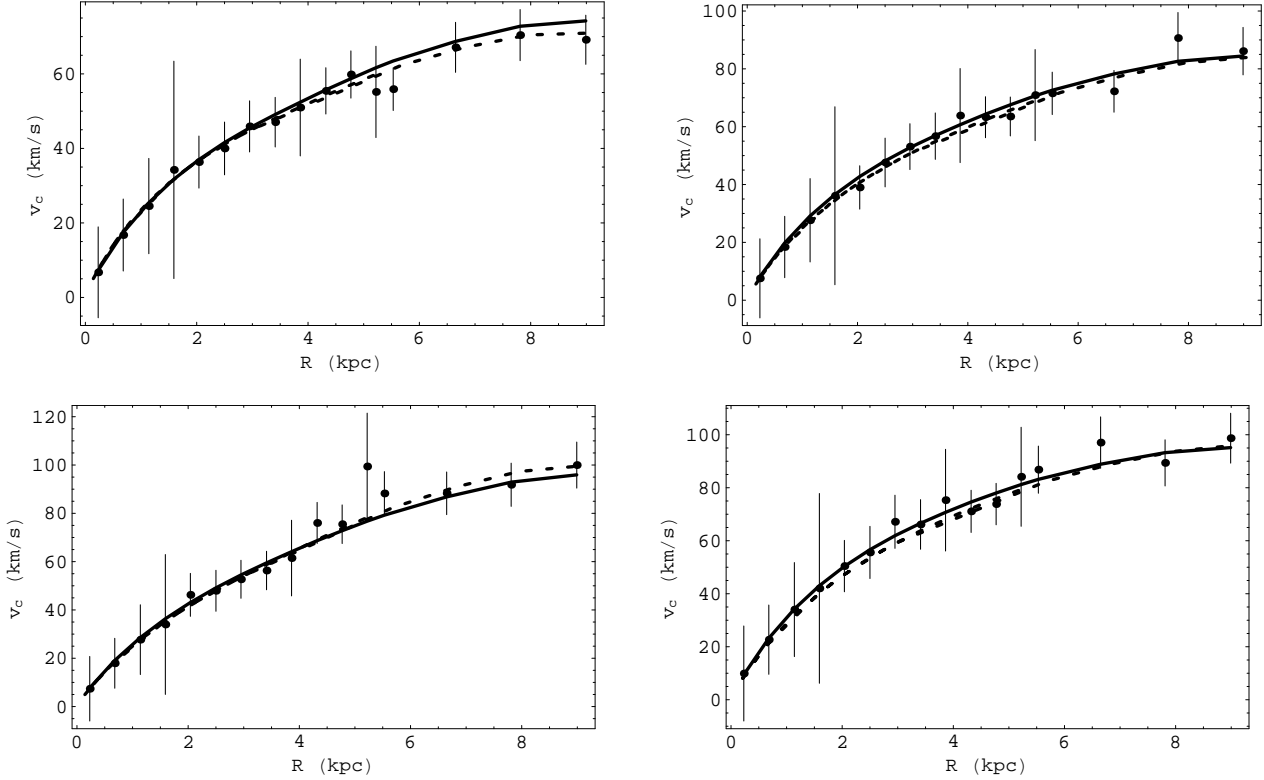


Figure 2. Some illustrative examples of simulated rotation curves (smoothing the data for convenience) with overplotted the input theoretical rotation curve (solid line) and the best fit one (short dashed line).

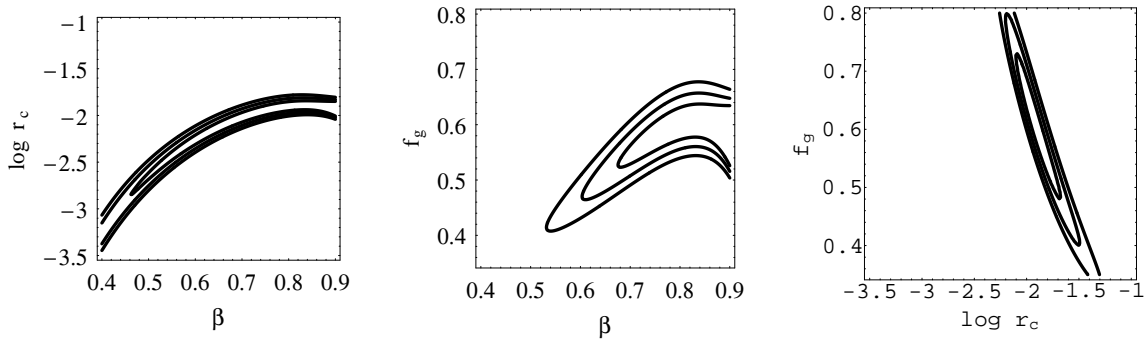


Figure 3. Contours of equal $\Delta\chi^2 = \chi^2 - \chi_{min}^2$ projected on the three planes $(\beta, \log r_c)$, (β, f_g) , $(\log r_c, f_g)$ for the case of the simulation in the top right panel of Fig. 2 with r_c in kpc. In each panel, the remaining parameter is set to its best fit value. The three contours individuate the 1, 2 and 3σ confidence ranges. Open contours mean that no constraints may be obtained.

line) are superimposed to the simulated data. Note that we plot smoothed rather than raw data in order to not clutter the graphic with too many points, but the raw data have been used in the fit. Although the two lines in each panel are always remarkably close so that they can be hardly discriminated by the data, the offset $\Delta p/p = |1 - p_{fit}/p_{sim}|$ may be quite large. Considering, for instance, the parameter β , we get $\Delta\beta/\beta = 24\%$, 11% , 17% and 16% from top left to bottom right clockwise respectively. Similar results are obtained for the full set of simulations, while smaller values of $\Delta p/p$ come out for $p = \log r_c$ and $p = f_g$ (and hence for Υ_*). It is also worth stressing that no significant correla-

tion has been observed between $\Delta p/p$ and p whatever is the parameter p considered.

This exercise also teaches us an important lesson. As it is apparent, better quality data could not be sufficient to break the degeneracy. An instructive example is represented by the top right panel where the two curves almost perfectly overlap. It is clear that reducing the error bars does not help at all so the input and the best fit models are impossible to discriminate notwithstanding a remarkable $\Delta\beta/\beta = 11\%$. In some cases, the two curves start departing from each other for large R so that one could expect that adding more points in this region or extending the data to still higher R effi-

ciently breaks the degeneracy. Unfortunately, the simulated data extend up to $\sim 5R_d$ so that further increasing this coverage with real data is somewhat unrealistic (especially using typical spiral galaxies rather than the gas rich LSBs).

The degeneracy hinted above among the model parameters also dramatically affects the estimated errors on $(\beta, \log r_c, f_g)$. This can be seen in Fig. 3 where we report the contours of equal $\Delta\chi^2$ projected on the three planes $(\beta, \log r_c)$, (β, f_g) , $(\log r_c, f_g)$ for the case of the simulation in the top right panel of Fig. 2. As it is clearly seen, β remains essentially unconstrained, while $\log r_c$ and f_g are only weakly constrained with the 3σ contours still spanning almost the full physical range for f_g . As suggested by the analysis of the pointlike case, these discouraging results are an expected consequence of the dependence of the theoretical rotation curve on the two degenerate quantities $(m_{eff}, r_{c,eff})$ preventing us to efficiently constraint separately the three model parameters.

5.2 Breaking the degeneracy among $(\beta, \log r_c, f_g)$

The analysis carried out convincingly shows that the degeneracy among the model parameters can not be broken by the present data on the rotation curves alone. As a result, one has to add some more constraints coming from different sources in order to set one of the three parameters above thus breaking the degeneracy and correctly recovering the values of the remaining two. Again, the analysis of the simulated rotation curves may help in choosing the best strategy.

As a first possibility, one may resort to stellar population synthesis models in order to set the M/L ratio Υ_* and hence the gas mass fraction f_g . Although this strategy is not free of problems (see the discussion in Sect. 6), one can ideally correlate the observed colors of the galaxy to the predicted M/L ratio and hence performing the fit to the data with the parameter f_g obtained by Eq.(39) so that $(\beta, \log r_c)$ are the only unknown quantities. The fit results to the full set of simulated rotation curves unequivocally show us that this strategy does not work at all. Although we do not report any illustrative examples, we warn the reader that quite similar plots to Fig. 2 are obtained. Actually, while $|\Delta \log r_c / \log r_c|$ is reduced to $\sim 10\%$, we still have $|\Delta \beta / \beta| \sim 20\%$ with values as high as 40%. Nevertheless, the input theoretical and the best fit rotation curves overlaps quite well over the range probed by the data.

As in the case with all the parameters free to vary, reducing the errors bars or extending the radial coverage is typically not sufficient for lowering $\Delta \beta / \beta$. Such a result may be anticipated by considering again Eq.(41). Setting Υ_* is the same as choosing m so that one could argue that $(\beta, \log r_c)$ may be determined by the effective quantities $(m_{eff}, r_{c,eff})$ that are constrained by the data. Actually, the situation is much more involved. Indeed, for $\beta \ll 1$, we are in a quasi Newtonian regime so that $r_{c,eff}$ is very weakly constrained and hence neither β nor r_c may be recovered. On the other hand, if $\beta \simeq 1$ the correction is small and again the constraints on both parameters are weak.

The simple exercise discussed above shows us that also a perfect knowledge of Υ_* is unable to break the remaining degeneracy between β and $\log r_c$ thus preventing the fit to recover their correct value. As a second possibility, one may resort to the theory itself and decide to set β from the

beginning. Actually, this is the same as setting the slope n of the R^n gravity Lagrangian. Since this latter must be the same from the galactic up to the cosmological scales, one may determine n from a different test and then set β from Eq.(15). The fit to the data may then be used to estimate $(\log r_c, f_g)$ which, on the contrary, depend on the particular system under examination. Indeed, we find that this strategy works very well. Both $\log r_c$ and f_g are recovered with great accuracy being $|\Delta \log r_c / \log r_c| \sim |\Delta f_g / f_g| \sim 5\%$ and never greater than $\sim 10\%$. Two cases representative of our best and worst situations are shown in Fig. 4. In both cases, the input theoretical curve and the best fit one may be hardly distinguished and indeed we get $(\Delta \log r_c / \log r_c, \Delta f_g / f_g) = (-2\%, -3\%)$ for the case in the left panel and $(3\%, 5\%)$ for the one in the right panel.

Considering the intrinsic errors induced by the displacement from the input rotation curve induced by our procedure used to generate the simulated data, we can safely conclude that both $\log r_c$ and f_g are exactly recovered within the expected precision.

It is also interesting to look at the bottom panels in Fig. 4 showing the iso- $\Delta\chi^2$ contours in the plane $(\log r_c, f_g)$. Although still covering a large region of the parameter space, the confidence ranges are now closed so that it is possible to extract meaningful constraints on the parameters. Following the usual approach (see, e.g., (de Blok & Bosma 2002)), 1 and 2 σ errors are obtained by projecting on the axes the contours for $\Delta\chi^2 = 1$ and $\Delta\chi^2 = 4$ respectively^{††}. A naive propagation of errors on f_g and the use of Eq.(39) makes it possible to infer constraints on Υ_* . It is remarkable that the uncertainty on $\log r_c$ remains large (hence rendering r_c known only within an order of magnitude). Reducing the error on $\log r_c$ is, however, quite difficult with the data at hand. As can be easily checked, r_c mainly determines the value of the circular velocity in the outer region with v_c being larger for smaller r_c . For $\beta \simeq 0.8$ as we will adopt later, $(r/r_c)^\beta \simeq 1 - 50$ for r ranging from 10^{-2} to $10^2 r_c$ where most of the data are concentrated. In order to get smaller errors on $\log r_c$, one should increase the number of points (and reducing the measurement uncertainties) in the region $r > 10^3 r_c$. For typical values of $\log r_c \simeq -2$ and $R_d \simeq 2$ kpc, one then needs to measure the rotation curve beyond $r \sim 5R_d$ which is quite unrealistic at the moment.

5.3 Raw vs smooth data

In the analysis of the simulated cases described above, we have up to now used the raw data as input to the fitting procedure. Nevertheless, in Sect. 4, we have claimed that the smooth rather than the raw data will be used in the analysis of the observed LSB galaxies rotation curves. As explained above and further discussed in de Blok & Bosma (2002) and references therein, smooth data are better suited to recover constraints on a given theory since they are less sensitive to non axisymmetric features and outliers affected by unpredictable errors.

^{††} We caution the reader that the contours in Figs. 3 and 4 refer to 2D confidence ranges so that $\Delta\chi^2 = 2.30, 6.17, 11.8$ respectively. They do not must be confused with those reported in the text which refer to constraints in a 1D parameter space.

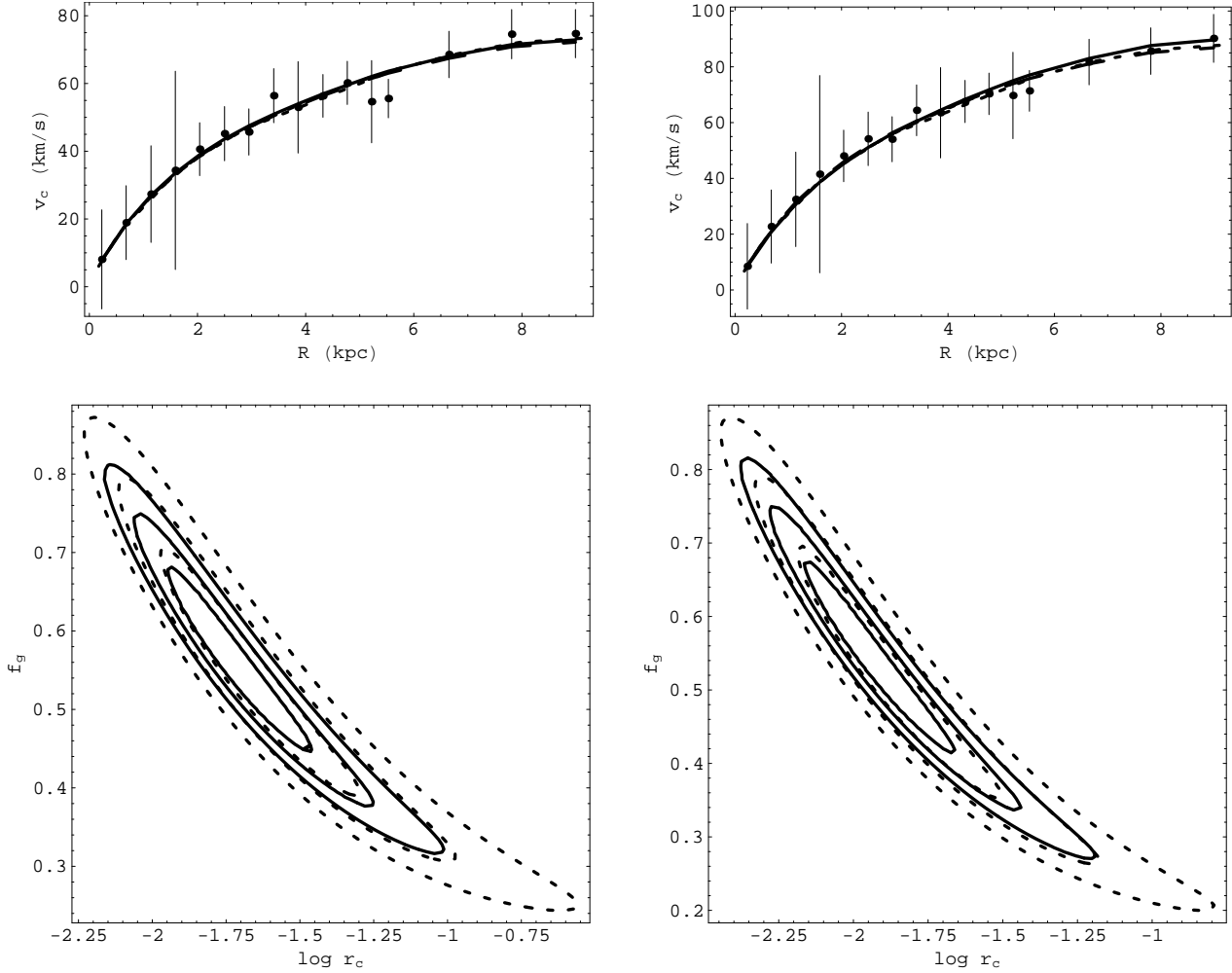


Figure 4. *Top panels.* Some illustrative examples of simulated rotation curves (smoothing the data for convenience) with overplotted the input theoretical rotation curve (solid line) and the best fit one from raw (short dashed line) and smooth (long dashed line) data. *Bottom panels.* 1, 2 and 3σ confidence ranges in the plane $(\log r_c, f_g)$ from the fit to raw (solid line) and smooth (short dashed line) data shown in the respective top panels (with r_c in kpc). Note that the two cases reported are representatives of the best (left) and worst (right) situations we find in our sample of simulated rotation curves.

Any smoothing procedure may potentially introduce some correlation among the data points because of binning the data and averaging the measurements in a given bin. Although the procedure adopted by de Blok & Bosma (2002) and briefly described in Appendix B is quite efficient in reducing these problems, a residual correlation still remains so that it is worth exploring whether this affects the results.

To this aim, we have fitted both the raw and the smooth data with the β parameter set for the reasons discussed above. As a first qualitative test, we have checked that the results are interchangeable, i.e. we may fit equally well the raw data with the best fit curve from the fit to the smooth data and vice versa. This is clearly seen in the top panels of Fig. 4 where the long dashed lines (representing the best fit to the smooth data) are hardly distinguished by the short dashed ones (from the fit to the raw data). As a more rigorous test, we have compared the best fit values from the two fits with those used to generate the simulated curve. Indeed, we find a remarkable agreement between the three

sets of $(\log r_c, f_g)$ values. What is more interesting, in many cases, $(\Delta p/p)_{smooth} < (\Delta p/p)_{raw}$ thus advocating in favor of the use of the smooth rather than the raw data.

As a final test, we also explore whether the confidence ranges and hence the uncertainties on the model parameters are affected. A nice visual result may be gained looking at the bottom panels in Fig. 4 and comparing the solid with the short dashed lines. As it is clear, the confidence regions quite well overlap with no visible offset from one another. Actually, using smooth rather than raw data leads to wider confidence regions and hence larger errors on $(\log r_c, f_g)$. However, this is expected since the smooth dataset contains a lower number of points so that we can roughly expect that the error σ_p on a parameter p increases by a factor $\varepsilon \propto (N_{raw}/N_{smooth})^{1/2}$. This is indeed the case when comparing the estimated errors from projecting the 1D confidence regions on the $(\log r_c, f_g)$ axes.

A final comment is in order. Because of how the measurement uncertainties have been computed, the best fit re-

duced $\chi^2/d.o.f$ values are not expected to be close to 1. This is indeed the case when dealing with the raw data. However, a further reduction is expected for the smooth data because of the peculiarities of the smoothing procedure used. For instance, we get $(\chi^2/d.o.f.)_{raw} = 0.29$ vs $(\chi^2/d.o.f.)_{smooth} = 0.07$ for the case in the right panel of Fig. 4. There are two motivations concurring to the finding of such small reduced χ^2 . First, the uncertainties have been conservatively estimated so that the true ones may also be significantly smaller. Should this be indeed the case, $\chi^2/d.o.f$ turn out to be underestimated. A second issue comes from an intrinsic feature of the smoothing procedure. As discussed in Appendix B, the method we employ is designed to recover the best approximation of an underlying model by a set of sparse data. Since the fit to the smooth data searches for the best agreement between the model and the data, an obvious consequence is that the best fit must be as close as possible to data that are by their own as close as possible to the model. As such, if the best fit model reproduces the data, the χ^2 is forced to be very small hence originating the observed very small values of the reduced χ^2 . Note that both these effects are systematics so that they work the same way over the full parameters space. Since we are interested in $\Delta\chi^2$ rather than χ^2_{min} , these systematics cancel out thus not affecting anyway the estimate of the uncertainties on the model parameters.

6 RESULTS

The extensive analysis of the previous section make it possible to draw two summarizing conclusions. First, we have to set somewhat the slope n of the gravity Lagrangian in order to break the degeneracy the model parameters. Second, we can rely on the smoothed data without introducing any bias in the estimated parameters or on their uncertainties.

A key role is then played by how we set n and hence β . To this aim, one may resort to cosmology. Indeed, R^n gravity has been introduced as a possible way to explain the observed cosmic speed up without the need of any dark energy component. Motivated by the first encouraging results, we have fitted the SNeIa Hubble diagram with a model comprising only baryonic matter, but regulated by modified Friedmann equations derived from the R^n gravity Lagrangian. Indeed, we find that the data are consistent with the hypothesis of no dark energy and dark matter provided $n \neq 1$ is assumed (Capozziello, Cardone and Troisi 2006). Unfortunately, the constraints on n are quite weak so that we have decided to set n to its best fit value without considering the large error. This gives $\beta = 0.817$ that we will use throughout the rest of the paper. Note that Eq.(15) quickly saturates as function of n so that, even if n is weakly constrained, β turns out to be less affected.

A comment is in order here. Setting β to the value derived from data probing cosmological scales, we are implicitly assuming that the slope n of the gravity Lagrangian is the same on all scales. From a theoretical point of view, this is an obvious consistency assumption. However, it should be nicer to derive this result from the analysis of the LSB rotation curves since they probe a different scale. Unfortunately, the parameters degeneracy discussed above prevents us to efficiently perform this quite interesting test. Indeed,

an accurate estimate of n from β needs a well determined β since a small offset $\Delta\beta/\beta$ translates in a dramatically large $\Delta n/n$. As a consequence, a possible inconsistency among the estimated β from different galaxies could erroneously lead to the conclusion that the gravity theory is theoretically not self consistent. To validate such a conclusion, however, one should reduce $\Delta\beta/\beta$ to less than 5%. Unfortunately, our analysis of the simulated rotation curves have shown us that this is not possible with the data at hand. It is therefore wiser to opt for a more conservative strategy and look for a consistency^{††} between the results from the cosmological and the galactic scales exploring whether the value of β set above allows to fit all the rotation curves with physical values of the remaining two parameters ($\log r_c, f_g$). This is our aim in this paper, while the more ambitious task hinted above will need for a different dataset.

With this caveat in mind, all we need to fit the data is the modelling of LSB galaxies described in Sect. 4.3 and the smoothed data available in literature. The best fit curves thus obtained are shown in Fig. 5, while the constraints on $(\log r_c, f_g)$ and on the stellar M/L ratio Υ_* are reported in Table 2. As a preliminary remark, it is worth noting that three galaxies (namely, NGC 2366, NGC 4395 and DDO 185) may be excluded by further discussion because of problematic data.

Indeed, for NGC 2366 the lack of data in the intermediate region prevents from deriving useful constraints, while the bump and the sink in NGC 4395 clearly signals the effect of local clumps in the gas distribution. Finally, for DDO 185, we have only 8 points separated by a large gap so that the fit is unable to converge. We stress that these cases are problematic whatever is the mass model and the gravity theory adopted so that we will not consider them anymore in the following discussion. A detailed case-by-case analysis of the full sample is presented in Appendix A, while here we mainly dedicate to some general lessons we can draw from the fit results.

Fig. 5 shows that, for 11 over 12 cases (the only problematic one being UGC 3137), there is an overall very good agreement between the data and the best fit curve thus suggesting that our modified gravitational potential allows to fit the data without any dark matter halo. Indeed, our model galaxies are based only on what is directly observed (the stellar mass and the gas content) and no exotic component is added. Needless to say, this is not possible in the standard Newtonian theory of gravity, while it is the presence of the additive power law term in the modified gravitational potential that makes it possible to increase the rotation curve in such a way to reproduce what is measured. In order to further substantiate this result, we can compare the constraints on the galactic parameters f_g and Υ_* with what is expected from astrophysical considerations.

First, we consider the gas mass fraction f_g . Roughly av-

^{††} A similar problem also arises when dealing with MOND where the critical acceleration a_0 plays a similar role as n for our theory. In principle, one should leave this quantity free when fitting galactic rotation curves and then check whether the same value is recovered for all galaxies. Unfortunately, model degeneracies prevent to perform such a test so that it is common to set a_0 to its fiducial value $1.2 \times 10^{-10} \text{ m/s}^2$ from the beginning.

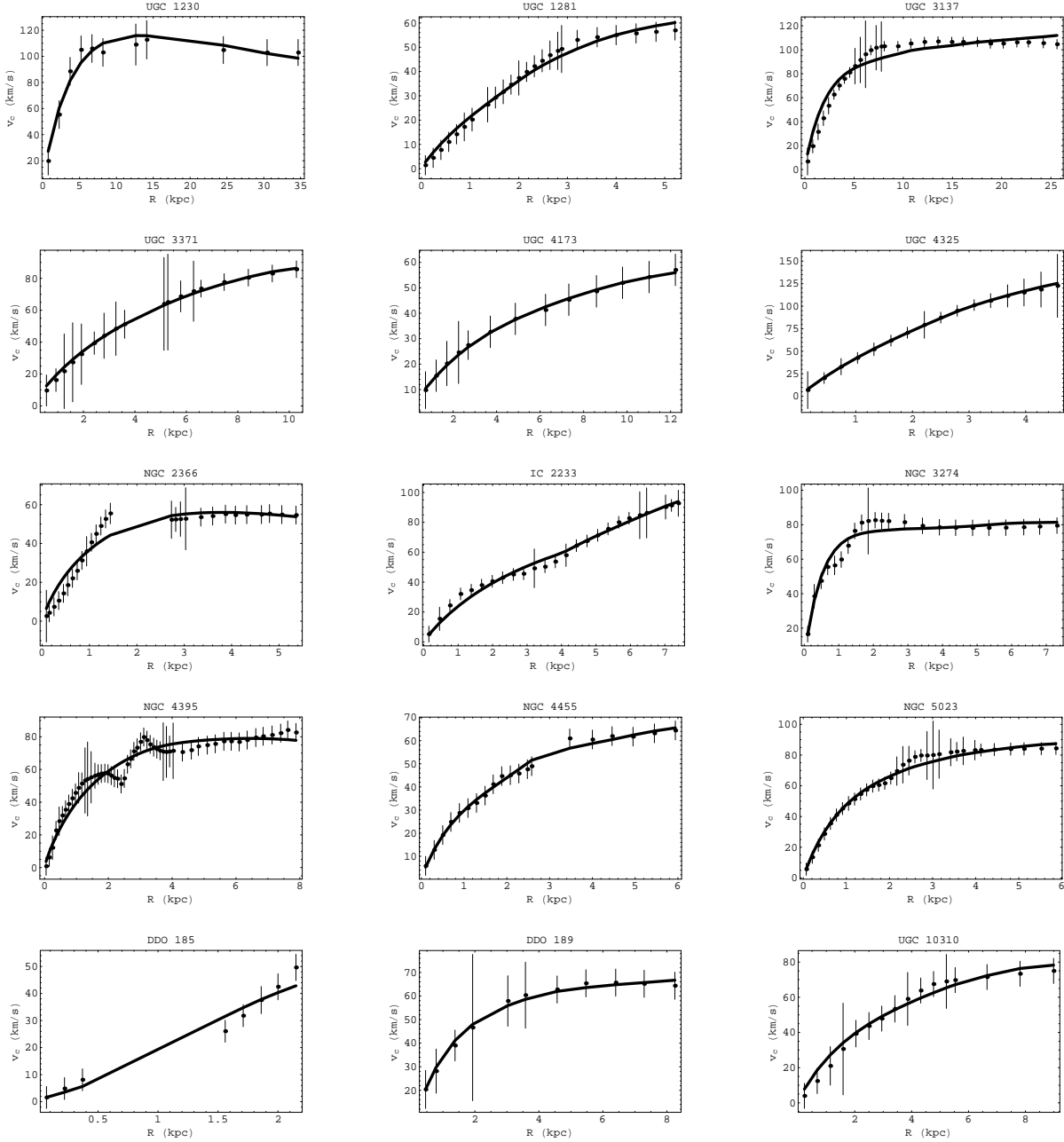


Figure 5. Best fit curves superimposed to the data for the sample of 15 LSB galaxies considered. See Table 1 for details on the galaxies and Table 2 for the values of the best fit parameters. A case by case discussion is presented in the Appendix A.

eraging the best fit values for the 11 successfully fitted galaxies, we get $\langle f_g \rangle \simeq 0.51$ with a standard deviation $\sigma_g \simeq 0.18$. Both these values are typical of LSB galaxies thus suggesting that our model galaxies are physically reasonable. As a further check, one could question whether the estimated values of the M/L ratio Υ_* are reasonable. The stellar M/L is usually obtained by fitting the Newtonian rotation curve of the exponential disk to the observed data in the inner region. However, such an estimate may be seriously biased. On the one hand, one usually add a dark halo contributing also to the inner rotation curve so that less disk mass is needed and hence the M/L ratio could be underestimated. On the other hand, being r_c of order 10^{-2} kpc, using the Newtonian

gravitational potential significantly underestimates the *true* rotation curve for a given disk mass so that more mass and hence an artificially higher M/L is needed if the halo is neglected. As a consequence, we cannot rely on the estimates of M/L reported in literature if they have been obtained by studying the inner rotation curve. A possible way out could be to use the relation between broad band colors and M/L (Bell & de Jong 2001). Unfortunately, this relation has been obtained by considering stellar population models that are typical of high surface brightness galaxies that have quite different properties. Moreover, such a relation has been calibrated by fitting the Tully-Fisher law under the hypothesis of maximal disk and Newtonian gravi-

Table 2. Best fit values of the model parameters from minimizing $\chi^2(\beta, \log r_c, f_g)$ with $\beta = 0.817$ corresponding to $n = 3.5$ as obtained from the best fit to the SNeIa data with only baryonic matter. We report 1σ (2σ) confidence ranges on the fitting parameters computed by projecting on the $(\log r_c, f_g)$ axes the contours $\Delta\chi^2 = 1$ ($\Delta\chi^2 = 4$). The best fit stellar M/L ratio Υ_* has been obtained evaluating Eq.(39) for the best fit f_g , while the uncertainty is obtained by usual propagation of errors symmetrizing the 1σ range of f_g . Note that this procedure is not completely correct since the errors are not Gaussian so that they are likely to be overestimated (especially when giving rise to unphysical negative lower limits for Υ_*). We also give $\chi^2/d.o.f.$ for the best fit model.

Id	$\log r_c$			f_g			Υ_*	χ^2/dof
	<i>bf</i>	1σ	2σ	<i>bf</i>	1σ	2σ		
UGC 1230	-0.38	(-0.59, -0.13)	(-0.78, -0.05)	0.15	(0.13, 0.18)	(0.10, 0.21)	$15.9 \pm 3.1 \pm 7.1$	0.33
UGC 1281	-2.12	(-2.26, -1.95)	(-2.38, -1.76)	0.47	(0.37, 0.56)	(0.29, 0.66)	$1.36 \pm 0.53 \pm 1.04$	0.22
UGC 3137	-1.67	(-1.70, -1.63)	(-1.73, -0.60)	0.61	(0.59, 0.63)	(0.57, 0.64)	$12.0 \pm 0.9 \pm 1.8$	1.80
UGC 3371	-1.78	(-1.99, -1.52)	(-2.16, -1.21)	0.40	(0.28, 0.54)	(0.20, 0.67)	$3.5 \pm 1.9 \pm 3.8$	0.03
UGC 4173	-0.74	(-1.11, -0.16)	(-1.39, 0.55)	0.36	(0.26, 0.49)	(0.20, 0.65)	$8.9 \pm 5.1 \pm 11.3$	0.01
UGC 4325	-2.81	(-2.96, -2.62)	(-3.07, -2.36)	0.69	(0.55, 0.80)	(0.40, 0.89)	$0.51 \pm 0.33 \pm 0.69$	0.01
NGC 2366	0.03	(-0.47, 1.05)	(-0.77, 1.25)	0.18	(0.17, 0.20)	(0.15, 0.23)	$14.4 \pm 1.9 \pm 4.4$	1.09
IC 2233	-2.05	(-2.12, -1.96)	(-2.19, -1.87)	0.60	(0.55, 0.64)	(0.50, 0.68)	$1.56 \pm 0.29 \pm 0.60$	0.50
NGC 3274	-2.09	(-2.14, -2.03)	(-2.19, -1.98)	0.49	(0.47, 0.52)	(0.44, 0.55)	$2.89 \pm 0.30 \pm 0.60$	0.84
NGC 4395	-0.25	(-0.50, -0.05)	(-0.69, 0.23)	0.093	(0.090, 0.101)	(0.088, 0.110)	$12.1 \pm 1.6 \pm 2.5$	0.70
NGC 4455	-2.36	(-2.41, -2.30)	(-2.46, -2.24)	0.85	(0.82, 0.87)	(0.79, 0.89)	$0.38 \pm 0.08 \pm 0.17$	0.18
NGC 5023	-2.52	(-2.58, -2.46)	(-2.63, -2.40)	0.52	(0.49, 0.55)	(0.46, 0.58)	$1.02 \pm 0.12 \pm 0.26$	0.29
DDO 185	-2.74	(-2.81, -2.52)	(-2.87, -2.10)	0.94	(0.71, 0.97)	(0.41, 1.00)	$0.12 \pm 0.49 \pm 1.14$	0.83
DDO 189	-1.82	(-1.85, -1.47)	(-2.00, -1.24)	0.53	(0.43, 0.62)	(0.35, 0.72)	$6.44 \pm 2.52 \pm 4.90$	0.06
UGC 10310	-1.76	(-1.92, -1.56)	(-2.05, -1.34)	0.56	(0.46, 0.65)	(0.37, 0.74)	$1.55 \pm 0.60 \pm 1.16$	0.21

tational potential. Indeed, as a cross check, we have used the Bell & de Jong (2001) formulae with the colors available in the NED database^{§§} obtaining values of Υ_* typically much smaller than 1. This is in contrast with the usual claim that $M/L \simeq 1.4$ for LSB galaxies (de Blok & Bosma 2002), while some suitably chosen population synthesis models predict Υ_* between 0.5 and 2 (van den Hock et al. 2000).

Excluding the four problematic galaxies (UGC 3137, NGC 2366, NGC 4395, DDO 185), a direct comparison of the values of Υ_* in Table 2 with the fiducial range (0.5, 2.0) shows that in 9 over 11 cases the fitted Υ_* is consistent within 1σ with the fiducial range quoted above. For UGC 1230 and DDO 189, the fitted M/L is unacceptably high so that a residual matter component seems to be needed. Should this missing matter be indeed dark matter, our proposed scenario would fail for these two galaxies. Deferring to Appendix A possible solutions for each single case, we here note that our constraints on Υ_* comes from those on f_g through Eq.(39). Here, an assumption on the helium fraction f_{He} has been assumed to convert the measured HI mass M_{HI} into the total gas mass $M_g = f_{He}M_{HI}$. Although reasonable, our choice for the constant conversion factor is affected by an unknown uncertainty that we have not taken into account. Moreover, we have assumed the same f_{He} for all galaxies, while it is conceivable that star evolution related phenomena could make f_{He} mildly galaxy dependent. Should f_{He} be lower, than Υ_* will be smaller thus lowering the disagreement observed. Moreover, we have not included any molecular gas in the gas budget. Although this is typi-

cally a good assumption, it is worth noting that our modified potential may increase the contribution to the total rotation curve of any mass element so that it is possible that the missing matter in UGC 1230 and DDO 189 is represented by unaccounted molecular gas. However, even excluding these two galaxies, we end up with a conservative estimate of 10 over 12 successful fits with plausible astrophysical values of the fitted galactic parameters which is a satisfactory considering the paucity of the sample.

Finally, let us consider the results on $\log r_c$. Different from the case of β , r_c is not a universal constant. Nevertheless, considering the conservative sample of 9 successfully fitted galaxies (thus excluding UGC 1230, UGC 3137, NGC 2366, NGC 4395, DDO 185, DDO 189) and roughly averaging the best fit values, we get $(\log r_c) = -2.0 \pm 0.6$. The reasonably low scatter in $\log r_c$ may be qualitatively explained considering that r_c mainly determines the value of the terminal velocity in the rotation curve. Since this quantity has a low scatter for the sample of LSB galaxies we have used, it is expected that the same holds for $\log r_c$.

The constraints on $(\log r_c, f_g)$ summarized in Table 2 have been obtained for $\beta = 0.817$, consistent with the best fit n from the fit to SNeIa Hubble diagram. However, since the estimate of n is affected by a large uncertainty so that it is worth wondering how this impacts the results presented here. To this aim, we have repeated the fit for UGC 10310 for $n = 2.5$ ($\beta = 0.740$) and $n = 4.5$ ($\beta = 0.858$). For the best fit values, we get :

$$(\log r_c, f_g, \Upsilon_*) = (-1.85, 0.58, 1.42) \text{ for } \beta = 0.740 ,$$

$$(\log r_c, f_g, \Upsilon_*) = (-1.36, 0.41, 1.62) \text{ for } \beta = 0.858 ,$$

to be compared with $(\log r_c, f_g, \Upsilon_*) = (-1.76, 0.56, 1.55)$. As expected, increasing β , $\log r_c$ and f_g become smaller in order to give the same observed rotation curve, consistent with what expected from Fig. 1. Although the shift in the

^{§§} Note that these colors are typically in a different photometric system than that used by Bell & de Jong (2001). Although this introduces a systematic error, it is unlikely that this causes a significant bias in the estimated M/L . For details see the NED database (<http://nedwww.ipac.caltech.edu>).

best fit values is significant, the data do not still allow to draw a definitive conclusion. For instance, the 2σ confidence ranges for $\log r_c$ turn out to be:

$$\begin{aligned} (-2.16, -1.39) & \text{ for } \beta = 0.740 \\ (-2.05, -1.34) & \text{ for } \beta = 0.817 \\ (-2.04, -1.35) & \text{ for } \beta = 0.858 \end{aligned} \quad (42)$$

which are consistent with each other. Note that further increasing n have no significant effect on the estimate of the parameters since β quickly saturates towards its asymptotic value $\beta = 1$. We are therefore confident that, although the constraints on $(\log r_c, \beta)$ depend on β , our main results are qualitatively unaltered by the choice of n (and hence β).

It is also worth noting that the three values of β considered above all provide quite good fits to the observed rotation curve. This is not surprising given the data at hand and our analysis parameters degeneracies presented in Sect. 5. In order to constrain β from rotation curves leaving it as a free parameter in the fit, therefore, one could explore the possibility to performed a combined χ^2 analysis of the full set of rotation curves. This can eventually be complemented by adding a prior on β , e.g., from the cosmological constraints on n . Exploring this issue is outside our aims here, but should be addressed in a forthcoming paper.

Summarizing, the results from the fit and the reasonable agreement between the recovered Υ_* and that predicted from stellar population synthesis models make us confident that R^n gravity is indeed a possible way to fit the rotation curves of LSB galaxies using only baryonic components (namely, the stellar disk and the interstellar gas) thus escaping the need of any putative dark matter halo.

7 DISCUSSION AND CONCLUSIONS

Rotation curves of spiral galaxies have been considered for a long time the strongest evidence of the existence of dark matter haloes surrounding their luminous components. Notwithstanding the great experimental efforts, up to now there has never been any firm detection of such an exotic dark component that should make up these haloes. It is therefore worth wondering whether dark matter indeed exists or it is actually the signal of the need for a different gravitational physics.

Motivated by these considerations, we have explored here the case of R^n gravity. Since such theories have been demonstrated to be viable alternatives to the dark energy giving rise to scenarios capable of explaining the observed cosmic speed up, it is highly interesting to investigate their consequences also at galactic scales. To this aim, we have solved the vacuum field equations for power-law $f(R)$ theories in the low energy limit thus deriving the gravitational potential of a pointlike source. It turns out that both the potential and the rotation curve are corrected by an additive term scaling as $(r/r_c)^{\beta-1}$ with the scalelength r_c depending on the system physical features (e.g. the mass) and β a function of the slope n of the gravity Lagrangian. In particular, for $n = 1$, our approximated solution reduces to the standard Newtonian one. For $0 < \beta < 1$, the potential is still asymptotically vanishing, but the rotation curve is higher than the Newtonian one. These results still hold when we compute the corrected potential for extended systems with

spherical symmetry or thin disk configuration. As a result, we have argued that the rotation curve of spiral galaxies could be fitted using the luminous components only thus eliminating the need for dark matter.

In order to verify this hypothesis, we have considered a sample of 15 LSB galaxies with well measured combined HI and H α rotation curves extending far beyond the optical edge of the disk. Since these systems are usually claimed to be dark matter dominated, reproducing their rotation curves without the need of any dark matter halo would represent a significant evidence in favour of R^n gravity. Moreover, fitting to rotation curves allows in principle to constrain the theory parameters (β, r_c) and determine the M/L ratio of the stellar component. Unfortunately, extensive simulations have highlighted the need to set a strong prior on β (and hence n) to break the degeneracy among the three fitting parameters $(\beta, \log r_c, f_g)$. To this aim, we have resorted to the results of SNeIAa Hubble diagram fitting without dark matter and dark energy which shows that $n = 3.5$ reproduces the data without the need of any dark sector.

Motivated by this consideration, we have set $n = 3.5$ giving $\beta = 0.817$ in order to check whether R^n gravity may fit both the SNeIa Hubble diagram and the LSB rotation curves without either dark energy on cosmological scales and dark matter on galactic scales with the same value of the slope n . Indeed, we conservatively estimate that 10 of a sample of 12 usable galaxies can be properly fitted by the corrected rotation curves based only on the baryonic components (stars and gas) of the galaxies with values of the M/L ratio which may be reconciled with predictions from stellar population synthesis models. It is worth emphasizing that all the LSB rotation curves have been successfully fitted using the same value of β . Although β has been set from the beginning, this does not guarantee that the full set of curves will be satisfactorily well fitted. Indeed, should we have found that a single rotation curve demands for a different β , this could have been a decisive evidence against R^n gravity. On the contrary, the same β leads to equally good fit for all the 10 successful galaxies. We therefore conclude that the self consistency of the theory has been verified thus leading further support to R^n gravity as a viable alternative to the dark sector on galactic and cosmological scales.

These encouraging results are a strong motivation for investigating R^n gravity further from both observational and theoretical point of views. Still remaining on galactic scales, it is mandatory to extend the analysis of the rotation curves to the case of high surface brightness (HSB) galaxies. Although their structure is more complicated (since one has to include also a bulge component), HSB galaxies are more numerous than LSB ones so that we may perform our test on a larger sample thus increasing the significance of the results. To this aim, it is important to carefully select the sample in order to include systems with well measured and extended rotation curve and not affected by possible non circular motions due to spiral arms or bar-like structures. While this could be a limitation, it is worth stressing that in modeling HSB one may neglect the gas component which has been the most important source of theoretical uncertainty in our study of LSB galaxies. Should the test on HSB be successful as the present one, we could convincingly demonstrate that R^n gravity is a *no dark matter* solution to the long standing problem of the rotation curves of spiral galaxies.

As well known, dark matter is invoked also on larger than galactic scales. For instance, dark matter haloes are typically present in clusters of galaxies and enter in a crucial way in determining the gas temperature profile which is measured from the X-ray emission. In such a case, the form of the gravitational potential plays a key role so that it is worth investigating whether our modified potential could reproduce the observed temperature profile without the need of dark matter. This test should also represent a further check of the consistency of the theory since it allows a determination of β on a completely different scale. Of course, one should find the same β , while a significant difference could be a clear signal of unescapable problems. Note that there are nowadays a large number of clusters whose gas temperature profiles is well measured thanks to the *Chandra* and *XMM-Newton* satellites so that also this test could be performed on a large sample to ameliorate the statistics.

A step further leads us to the cosmological scales where dark matter is introduced to fill the gap between the baryonic density parameter Ω_b and the estimated total matter one Ω_M . According to nucleosynthesis predictions, $\Omega_b = 0.0214 \pm 0.0020$ (Kirkman et al. 2003), while $\Omega_M \simeq 0.25$ is estimated by SNeIa Hubble diagram and matter power spectrum. Such a large discrepancy may seem to be impossible to cure without resorting to dark matter. However, this could also not be the case when considering that both the SNeIa Hubble diagram and the matter power spectrum are usually computed assuming General Relativity as the correct theory of gravity. However, should $f(R)$ theories be indeed the correct model, one should recompute *ab initio* the matter power spectrum so that it is impossible to predict *a priori* what is the value of Ω_M that allows a nice fit to the measured matter power spectrum in a higher order theory. There is therefore much room for further investigation and it is indeed possible that a baryons only universe is in agreement with the cosmological data if an alternative theory of gravity, instead of Einstein General Relativity, is used.

As a final comment, we would like to stress the power of an approach based on higher order theories of gravity. Although it is still possible that the choice $f(R) = f_0 R^n$ is unable to positively pass all the tests we have quoted above, it is important to note that $f(R)$ theories are the unique mechanism able to explain in a single theoretical framework physical phenomena taking place on widely different scales. In our opinion, therefore, if a unified solution of the dark matter and dark energy problems exist, this is the realm where it has to be searched for with the greatest chances of successful results.

Acknowledgements. We warmly thank M. Capaccioli for the interesting discussions and encouragements. We are also extremely grateful to W.J.G. de Blok for his prompt answers to the many questions on the data and the LSB modeling, to G. D'Agostini for an illuminating discussion on the use of marginalized likelihood functions and to F. Giubileo for help with data retrieving. We also thank G. Lambiase, C. Rubano and G. Scarpetta for discussions and comments on preliminary versions of the paper. Finally, the referee is greatly acknowledged for his suggestions that have helped to radically improve the paper.

APPENDIX A: DETAILS ON FIT RESULTS

In Sect. 6, we have discussed the main features of the fit results as a whole, while here we give some few details on the comparison of the model with the rotation curve on a case-by-case basis.

UGC 1230. This is a somewhat problematic case giving a best fit $\Upsilon_\star = 15.9 \pm 3.1$ which is hard to explain in terms of reasonable population synthesis models. High values of M/L are also obtained in the case of maximum disk and dark halo models. For instance, de Blok & Bosma (2002) find $\Upsilon_\star = 6.1$ for both isothermal and NFW dark halo models. It is therefore likely that a problem may reside in the data or in the modelling (e.g., an underestimate of the gas content or a wrong measurement of the distance of the galaxy that could lead to underestimate the total absolute luminosity and hence overestimating Υ_\star). Although such a possibility exist, it is worth noting that the value of $\log r_c$ is significantly larger than what is found for the other galaxies thus enhancing the need for an unseen component at odds with our working hypothesis of no dark matter. We have therefore decided to not consider UGC 1230 as a successful fits even if there is a good agreement between the data and the best fit curve.

UGC 1281. This is a typical case with the model nicely reproducing the data and a value of Υ_\star in agreement with population synthesis models. There is only a marginal overestimate of the rotation curve for $R \leq 1$ kpc, but it is well within the errors. To this aim, we remark that a slight overestimate of the theoretical rotation curve for the innermost points is expected for all galaxies since we have artificially assumed the gas surface density is flat in this region where no data are available. Should this not be the actual situation, v_c turns out to be slightly biased high.

UGC 3137. This case is not satisfactory for our approach. Indeed, the reduced χ^2 for the best fit model is anomalously high (~ 2) essentially due to the theoretical curve being higher than the observed one for the innermost points and smaller in the intermediate region. Moreover, the estimated $\Upsilon_\star = 12.0 \pm 1.9$ is too large to be reconciled with population synthesis models. The disagreement is hard to explain given that the data seem to be of good quality and the curve is quite smooth. It is, however, worth noting that it is not possible to achieve a good fit also in the dark matter case whatever is the halo model used (see, e.g., de Blok & Bosma 2002). It has to be remarked that UGC 3137 is an edge-on galaxy so that deriving a disk mass model from the surface brightness involves a series of assumptions that could have introduced some unpredictable systematic error.

UGC 3371. The agreement between the data and the model is extremely good and the estimated values of $(\log r_c, f_g)$ are typical of the sample we have considered. The best fit Υ_\star is somewhat larger than expected on the basis of stellar population model, but the fiducial $\Upsilon_\star = 1.4$ typically used in dark matter fitting is only 1σ smaller. We can therefore consider this fit successful and physically reasonable.

UGC 4173. Although the agreement between the data and the best fit model is almost perfect, this case is somewhat more problematic than UGC 3371 since we get an anomalously high Υ_* . As such, we could deem this galaxy as a failure for R^n gravity. However, examining the 2D confidence regions in the plane $(\log r_c, f_g)$, it is easy to find out models with typical values of $\log r_c$ and lower Υ_* that could still agree with the rotation curve within the errors. Moreover, the uncertainties on the data points are probably overestimated as could be inferred noting that also dark halo models reproduce the observed curve with a very small χ^2 which is a typical signal of too high errors. Given these issues, we include this galaxy in the sample of successful fits.

UGC 4325. The best fit model matches perfectly the observed rotation curve with a typical value of $\log r_c$, but a somewhat small but still reasonable Υ_* . However, since $\log r_c$ and Υ_* are positively correlated, one could increase $\log r_c$ and hence Υ_* still achieving a very good fit to the data, even if this is not our final choice.

NGC 2366. This curve is a challenge both for R^n gravity and dark matter models. The very linear rise in the inner part rapidly changes in a flat part at larger radii. Moreover, there are no points in the intermediate region that could give constraints on how the change takes place. As de Blok & Bosma (2002) suggests, it is possible that the outermost points which are based on the HI data alone are underestimated. Another possibility is the presence of non circular motions due to the inner bar-like structure. These uncertainties on the data lead to a very bad fit with large values for both $\log r_c$ and Υ_* . Given this situation, we have not considered anymore this galaxy stressing, however, that this is not an evidence against R^n gravity.

IC 2233. It is quite difficult to get a very good fit to this galaxy rotation curve since, looking at the plot, one sees an abrupt change of concavity for $R \geq 3$ kpc. As a consequence, a perfect matching between the data and the model is not possible. Nevertheless, the best fit model provides a quite good agreement with the data. Moreover, the best fit values of $(\log r_c, f_g)$ are typical of our sample and the estimated Υ_* nicely agrees with the fiducial one suggested in previous literature. We can therefore consider this galaxy as one of the most remarkable successes of R^n gravity.

NGC 3274. Although the general trend of the curve is well reproduced, there is a certain disagreement in the region $1 \text{ kpc} \leq R \leq 2 \text{ kpc}$ where a change of concavity occurs that is not reproduced by the model. Note that features like this could be related to a clumpiness in the gas distribution that cannot be modeled analytically. Considering, moreover, that the value of $\log r_c$ is quite typical and the estimated M/L ratio is not too difficult to reconcile with population synthesis models (although somewhat high), we conclude that R^n gravity successfully reproduces this curve.

NGC 4395. The rotation curve of this galaxy is strongly affected by the presence of star formation regions that cause an oscillating behaviour for $1.5 \text{ kpc} \leq R \leq 4 \text{ kpc}$ that is not possible to reproduce by any analytical model. Indeed, the best fit model is unable to agree reasonably well

with the data so that the results on $(\log r_c, f_g)$ are significantly altered. Given the problems with the modeling, we have therefore decided to exclude this galaxy from the final sample since it is impossible to decide whether a bad fit is a signal of a breakdown for R^n gravity.

NGC 4455. Both the fit and the estimated values of the model parameters are quite satisfactory, although the low Υ_* may argue in favour of a higher $\log r_c$. Note that there is a hole in the observed rotation curve around ~ 3 kpc. Adding some more data in this region could help in better constraining the parameters with particular regard to Υ_* . It is worth noting that the best fit curve tends to be higher (but well within the measurement errors) in the outer region. Extending the measurement of this galaxy rotation curve to larger radii could therefore be a crucial test for our paradigm in this particular case. Note, however, that it is also possible that the parameters will be adjusted in such a way to still provide a good fit.

NGC 5023. This edge-on galaxy is, in a certain sense, an ameliorated version of UGC 3137. Indeed, the best fit model underestimates the rotation curve in the region between 2 and 3 kpc, but fits quite well the remaining data. Inspecting the rotation curve, a change of concavity occurs at 2 kpc and it is, indeed, this feature the origin of the disagreement. The similarity with the case of UGC 3137 could suggest to reject this galaxy considering also this fit as an unsuccessful one. However, a closer look shows that, while in the case of UGC 3137 the best fit model works bad both in the inner and the intermediate regions, here the disagreement is limited to the zone where the change of concavity takes place. Moreover, in this case, the best fit $\log r_c$ is typical of our sample and the estimated M/L ratio is quite reasonable so that we have finally decided to retain this galaxy.

DDO 185. This very linear curve is quite difficult to reproduce and, indeed, our best fit model makes a poor job with a too small M/L ratio. However, the overall rotation curve measurements are of very poor quality so that this galaxy can be discarded from further considerations.

DDO 189. There is an almost perfect matching between the data and the best fit model. The estimated values of $(\log r_c, f_g)$ are typical for the LSB galaxies in our sample, but Υ_* is unexpectedly large. Since f_g takes a completely reasonable value, a possible problem could arise with the conversion from f_g to Υ_* . For instance, should f_{He} be smaller than our fiducial value, then Υ_* should be revised towards lower values. In order to be conservative, we have however decided to exclude this galaxy from the sample of successful fits even if nothing prevents the reader to take the opposite decision.

UGC 10310. Everything works well for this galaxy. The best fit model provides a good fit to the observed rotation curve with only a modest overestimate (still within the uncertainties) in the innermost region that could be ascribed to our assumptions in the gas modelling. The values of $\log r_c$ and f_g are typical of our sample, while the best fit Υ_* may be easily reconciled with the predictions from stellar population synthesis models.

APPENDIX B: SMOOTHING THE DATA

As input to the pipeline for testing R^n gravity, we have used the smoothed version of the rotation curve data following the same approach used by de Blok & Bosma (2002). As explained in Sect. 4, the use of the smooth rather than the raw data relies on the need to eliminate any residual effect of non circular motions on the data since the gas and disk mass models assume that these components are axisymmetric systems. However, the smoothing procedure may in principle introduce correlations among the data so that it is worth investigating whether this may bias somewhat the results on the model parameters. This task has been extensively performed in Sect. 5.3 so that here we only give some more details on how the smoothing is done referring to Loader (1999) and de Blok & Bosma (2002) for further details.

First, the data have been symmetrized and folded and then resampled each 6 arcsec. Since both HI and H α data are available, when there is an overlap, only H α points have been retained for $r \leq r_\alpha$ with the values of r_α available in Table 1 of de Blok & Bosma (2002). The smooth data have been obtained using a local regression method following the steps schematically sketched below.

- (i) Choose N points x_1, \dots, x_N .
- (ii) Define the weight function $w(u) = (1 - |u|^3)^3$ for $|u| \leq 1$, $w(u) = 0$ for $|u| > 1$, with $u = (x - x_i)/h$ being h the width of the bin centred on x_i .
- (iii) Given a set of N_{obs} observed points (x_j, v_j) , perform a weighted fit of the polynomial $\mathcal{P}_p = \sum_{l=0}^p a_l (x - x_i)^l$ to these data using the function $w(u)$ defined above to generate the weights.
- (iv) Estimate the smoothed value of the rotation curve in x_i as the zeroth order term of the polynomial fitted above.
- (v) Repeat this procedure for each one of the N points (x_1, \dots, x_N) thus ending with a smoothed rotation curve dataset made out of N points (x_i, v_i) .

It is worth stressing that this smoothing procedure introduces a negligible amount of correlations among the different points in the rotation curve. Indeed, the fit of the polynomial of degree p is performed only locally so that two consecutive bins have only a modest (if not null) number of points in common depending on the chosen value of h . As discussed in Loader (1999), local regression methods make it possible to recover the information about a given function eliminating the noise that affects the observed data. At the same time, being local, the regression method minimizes the correlations between the different bins.

As shown in Sect. 5.3, the best fit model passes almost perfectly within the simulated smoothed data yielding a very small χ^2 value. This is an expected consequence of the ability of local regression methods to recover the true model from noisy data. As such, if the fitted model reproduces the data, it is, in a certain sense, forced to pass almost exactly through the smoothed points since they represent the best approximation to the true underlying model. If the fit is successful, the true model and the best fit model coincide so that the χ^2 is expected to be very small.

REFERENCES

- Allemandi, G., Francaviglia, M., Ruggiero, M., Tartaglia, A. 2005, *Gen. Rel. Grav.*, 37, 1891
- Astier, P. et al. 2006, *A&A*, 447, 31
- Bachall, N.A., Bode, P. 2003, *ApJ*, 588, 1
- Bachall, N.A. et al. 2003, *ApJ*, 585, 182
- Bell, E.F., de Jong, R.S. 2001, *ApJ*, 550, 212
- Binney, J., Tremaine, S. 1987, *Galactic dynamics*, Princeton University Books, Princeton (USA)
- Borowiec, A., Godlowski, W., Szydowski, M. 2006, *Phys. Rev. D*, 74, 043502
- Brodbeck, O., Straumann, N. 1993, *J. Math. Phys.*, 34, 6
- Bronnikov, K., Melnikov, V. 1994, *Gen. Rel. Grav.*, 27, 465
- Capozziello, S. 2002, *Int. J. Mod. Phys. D*, 11, 483
- Capozziello, S., Cardone, V.F., Carloni, S., Troisi, A. 2003, *Int. J. Mod. Phys. D*, 12, 1969
- Capozziello, S., Cardone, V.F., Carloni, S., Troisi, A. 2004, *Phys. Lett. A*, 326, 292
- Capozziello, S., Cardone, V.F., Francaviglia, M. 2006, *Gen. Rel. Grav.*, 38, 711
- Capozziello, S., Cardone, V.F., Troisi, A. 2005, *Phys. Rev. D*, 71, 043503
- Capozziello, S., Cardone, V.F., Troisi, A. 2006, *JCAP*, 0608, 001
- Capozziello, S., Carloni, S., Troisi, A. 2003, *Rec. Res. Dev. Astronomy. & Astrophys.*, 1, 625, astro-ph/0303041
- Capozziello, S., Troisi, A. 2005, *Phys. Rev. D*, 72, 044022
- Carloni, S., Dunsby, P.K.S., Capozziello, S., Troisi, A. 2005, *Class. Quantum Grav.* 22, 2839
- Carroll, S.M., Duvvuri, V., Trodden, M., Turner, M.S. 2004, *Phys. Rev. D*, 70, 043528
- Carroll, S.M., Press, W.H., Turner, E.L. 1992, *ARA&A*, 30, 499
- Catinella, B., Giovanelli, R., Haynes, M.P. 2006, *ApJ*, 640, 751
- Cembranos, J.A.R. 2006, *Phys. Rev. D*, 73, 064029
- Chiba, T. 2003, *Phys. Lett. B*, 575, 1
- Clifton, T., Barrow, J.D. 2005, *Phys. Rev. D*, 72, 103005
- Clocchiati, A. et al. 2006, *APJ*, 642, 1
- Cole, S. et al. 2005, *MNRAS*, 362, 505
- Croft, R.A.C., Hu, W., Dave, R. 1999, *Phys. Rev. Lett.*, 83, 1092
- de Bernardis, P. et al. 2000, *Nature*, 404, 955
- de Blok, W.J.G., Bosma, A. 2002, *A&A*, 385, 816
- de Blok, W.J.G. 2005, *ApJ*, 634, 227
- Dick, R. 2004, *Gen. Rel. Grav.*, 36, 217
- Dolgov, A.D., Kawasaki, M. 2003, *Phys. Lett. B*, 573, 1
- Eisenstein, D. et al. 2005, *ApJ*, 633, 560
- Eke, V.R., Cole, S., Frenk, C.S., Petrick, H.J. 1998, *MNRAS*, 298, 1145
- Freeman, K. 1970, *ApJ*, 160, 811
- Kirkman, D., Tyler, D., Suzuki, N., O'Meara, J.M., Lubin, D. 2003, *ApJS*, 149, 1
- Kluske, S., Schmidt, H.J. 1996, *Astron. Nachr.*, 37, 337
- Loader, C. 1999, *Local regression and likelihood*, Springer - Verlag, New York
- McDonald, P. et al. 2005, *ApJ*, 635, 761
- Navarro, I., van Acoleyen, K. 2005, *Phys. Lett. B*, 622, 1
- Neville, D. 1980, *Phys. Rev. D*, 21, 10
- Nojiri, S., Odintsov, S.D. 2003, *Phys. Lett. B*, 576, 5
- Olmo, G.J. 2005, *Phys. Rev. D*, 72, 083505
- Padmanabhan, T. 2003, *Phys. Rept.*, 380, 235
- Peebles, P.J.E., Rathra, B. 2003, *Rev. Mod. Phys.*, 75, 559
- Persic, M., Salucci, P., Stel, F. 1996, *MNRAS*, 281, 27
- Pope, A.C. et al. 2005, *ApJ*, 607, 655
- Ramaswamy, S., Yasskin, P.B. 1979, *Phys. Rev. D*, 19, 2264
- Refregier, A. 2003, *ARA&A*, 41, 645
- Riess, A.G. et al. 2004, *ApJ*, 607, 665
- Sahni, V., Starobinski, A. 2000, *Int. J. Mod. Phys. D*, 9, 373
- Sanchez, A.G. et al. 2006, *MNRAS*, 366, 189

- Schmidt, H.J. 2004, *Lectures on mathematical cosmology*, gr-qc/0407095
- Schombert, J.M., McGaugh, S.S., Eder, J.A. 2001, *AJ*, 121, 2420
- Seljak, U. et al. 2005, *Phys. Rev. D*, 71, 103515
- Sobouti, Y. 2006, astro-ph/0603302
- Sofue, Y., Rubin, V. 2001, *ARA&A*, 39, 137
- Sotiriou, T.P. 2006, *Gen. Rel. Grav.*, 38, 1407
- Spergel, D.N. et al. 2003, *ApJS*, 148, 175
- Starobinsky, A.A. 1980, *Phys. Lett. B*, 91, 99
- Stelle, K.S. 1978, *Gen. Rel. Grav.*, 9, 353
- Tegmark, M. et al. 2004, *Phys. Rev. D*, 69, 103501
- van den Hock, L.B., de Blok, W.J.G., van der Hulst, J.M., de Jong, T. 2000, *A&A*, 357, 397
- van Waerbeke, L. et al. 2001, *A&A*, 374, 757
- Viana, P.T.P., Nichol, R.C., Liddle, A.R. 2002, *ApJ*, 569, 75